Serrage, H. J., FitzGibbon, L., Alibhai, D. R., Cross, S., Rostami, N., Jack, A. A., Lawler, C. R. E., Jakubovics, N. S., Jepson, M. A., & Nobbs, A. H. (2022). Quantification of Extracellular DNA Network Abundance and Architecture within Streptococcus gordonii Biofilms Reveals Modulatory Factors. *Applied and Environmental Microbiology*, *88*(13). https://doi.org/10.1128/aem.00698-22

Quantification of eDNA network abundance and architecture within *Streptococcus gordonii* biofilms reveals modulatory factors

Hannah J. Serrage,[a*] Dominic Alibhai,[b] Stephen Cross,[b] Nadia Rostami,[c] Alison A. Jack,[a*] Catherine R. E. Lawler,[a*] Nicholas S. Jakubovics,[c] Mark A. Jepson,[b] and Angela H. Nobbs[a#]

[a]Bristol Dental School, University of Bristol, Bristol, UK

[b]Wolfson Bioimaging Facility, Biomedical Sciences Building, University of Bristol, Bristol, UK

[c]School of Dental Sciences, Newcastle University, Newcastle upon Tyne, UK

Running title: eDNA modulation in *S. gordonii* biofilms

#Address correspondence to: Angela H. Nobbs, angela.nobbs@bristol.ac.uk

*Present address: Hannah J. Serrage, University of Manchester, Manchester, UK; Alison A. Jack, Life Sciences Hub Wales, Cardiff, UK; Catherine R. E. Lawler, University of Bath, Bath, UK.

Abstract

Extracellular DNA (eDNA) is an important component of biofilm matrix that serves to maintain biofilm structural integrity, promotes genetic exchange within the biofilm, and provides protection against antimicrobial compounds. Advances in microscopy techniques have provided evidence of the cobweb- or lattice-like structures of eDNA within biofilms from a range of environmental niches. However, methods to reliably assess the abundance and architecture of eDNA remain lacking. This study aimed to address this gap by development of a novel, high-throughput image acquisition and analysis platform for assessment of eDNA networks *in situ* within biofilms. Utilising *Streptococcus gordonii* as the model, the capacity for this imaging system to reliably detect eDNA networks and monitor changes in abundance and architecture (e.g., strand length, branch number) was verified. Evidence was provided of a synergy between glucans and eDNA matrices, while it was revealed that surface-bound nuclease SsnA could modify these eDNA structures under conditions permissive for enzymatic activity. Moreover, cross-talk between the competence and hexa-heptapeptide permease systems was shown to regulate eDNA release by *S. gordonii.* This novel imaging system can be applied across the wider field of biofilm research, with potential to significantly advance interrogation of the mechanisms by which the eDNA network architecture develops, how it can influence biofilm properties, and how it may be targeted for therapeutic benefit.

Importance

Extracellular DNA (eDNA) is critical for maintaining the structural integrity of many microbial biofilms, making it an attractive target for the management of biofilms. However, our knowledge and targeting of eDNA is currently hindered by a lack of tools for the quantitative assessment of eDNA networks within biofilms. Here, we demonstrate use of a novel image acquisition and analysis platform with the capacity to reliably monitor the abundance and architecture of eDNA networks. Application of this tool to *Streptococcus gordonii* biofilms has provided new insights into how eDNA networks are stabilised within the biofilm and the pathways that can regulate eDNA release. This highlights how exploitation of this novel imaging system across the wider field of biofilm research has potential to significantly advance interrogation of the mechanisms by which the eDNA network architecture develops, how it can influence biofilm properties, and how it may be targeted for therapeutic benefit.

Introduction

Biofilm development is characterised by the production and release of extracellular polymeric substance (EPS) to form a matrix that encases the microbial community. EPS accounts for >90% biofilm dry weight and comprises a rich tapestry of components including extracellular DNA (eDNA), which has been found as a common component of biofilms across a range of environments (1-3). Diverse roles have been ascribed to eDNA, including maintenance of biofilm structural integrity, facilitating initial adhesion to surfaces, acting as a reservoir for genetic exchange, providing protection against antimicrobial compounds, and as a nutrient source (4). As a consequence, eDNA is often considered an attractive target for the management of biofilms, which account for up to 80% of all nosocomial infections in humans (5).

Within the biofilm, eDNA is proposed to conform to an “electrostatic net” model where, under low pH conditions, negatively charged eDNA forms electrostatic interactions with positively charged DNA binding proteins within EPS, acting as a net that interconnects cells (6, 7). Advances in techniques for the visualisation of fluorescently stained eDNA networks have provided insights into their structural composition (8-10). Specifically, eDNA has been shown to form Holliday junction-like (9) and G-quadruplex structures (8), stabilised by DNA binding proteins (11-14), that ultimately form cobweb- or lattice-like networks across the biofilm (9, 10). However, understanding of the mechanisms by which eDNA is released, how this is regulated, and the spatiotemporal dynamics of eDNA network formation remains limited. This is, in part, driven by a lack of tools with

77 the capacity to reliably detect and quantify the abundance and architecture of eDNA
78 networks within biofilms.
79
80 One ecological niche in which eDNA is recognised as a prominent component of
81 biofilms and a promising therapeutic target is within the oral cavity and, specifically,
82 dental plaque. *Streptococcus gordonii* is a pioneer coloniser and ubiquitous constituent
83 of dental plaque biofilms, where it can influence the accretion of the dental plaque
84 community on salivary pellicle (3, 15). DNA extraction techniques that enable the
85 quantification of soluble eDNA have confirmed the capacity for *S. gordonii* to produce
86 eDNA during biofilm formation (16, 17). From such studies, *S. gordonii* eDNA is
87 hypothesised to be of chromosomal origin and its release has been shown to be
88 hydrogen peroxide (H_2O_2) dependent (16, 18). However, further insights into the
89 parameters that may affect *S. gordonii* eDNA networks and their overall architecture are
90 lacking.
91
92 Here we demonstrate use of a novel, high-throughput image acquisition and analysis
93 platform to reliably quantify the abundance and architecture of eDNA networks *in situ*
94 within early *S. gordonii* biofilms. By exploiting this technology, these studies provide
95 evidence of glucan stabilisation of the eDNA matrix, reveal that a surface-bound
96 nuclease can modulate the eDNA networks, and identify crosstalk between the
97 competence and hexa-heptapeptide permease (Hpp) systems in regulating eDNA
98 release. The high level detail of eDNA network analysis that this imaging system

provides has potential to significantly advance current understanding of biofilm development and manipulation across the spectrum of biofilm research.

Results

Evaluation of eDNA production in early-stage S. gordonii biofilms

Pilot studies had indicated the capacity for *S. gordonii* to produce an eDNA network during biofilm formation, alike in architecture to the yarn-like eDNA structures produced by *Enterococcus faecalis* biofilms (10). *S. gordonii* biofilms were therefore selected as the model to verify the capacity for our image analysis approach to reproducibly quantity eDNA networks *in situ* within biofilms. Before such studies could be undertaken, however, it was necessary to establish the optimal stage during biofilm development at which *S. gordonii* produces eDNA. Previous reports had indicated that *S. gordonii* releases eDNA during early biofilm formation (16, 17) but detailed, time dependent changes in eDNA release were lacking. Phenol:chloroform:isoamyl DNA extraction was combined with crystal violet staining to systematically evaluate changes in soluble eDNA and biomass quantities over time. A time-dependent increase in eDNA concentration was seen that peaked at 5 h and then began to decline, while biomass levels continued to increase beyond 5 h (Fig. 1). This indicated that eDNA levels did not simply correlate with *S. gordonii* cell numbers. As it represented the peak for eDNA concentration, a 5-h time point was selected to further evaluate eDNA within *S. gordonii* biofilms.

Quantification of eDNA networks within S. gordonii biofilms

The quantification of DNA by phenol:chloroform:isoamyl alcohol extraction has been used widely to quantify levels of eDNA within biofilms (31-33). However, this approach only indicates the concentration of soluble eDNA and can provide no information on the structural complexity of eDNA within the biofilm architecture. To address this limitation, a novel mass image acquisition and high-throughput image analysis system was devised to both visualise and quantify eDNA networks *in situ* within biofilms. Immunolabelling of double-stranded eDNA combined with TO-PRO-3 staining of *S. gordonii* cells revealed web- or constellation-like networks of eDNA extending across the *S. gordonii* biofilm (Fig. 2). Our image analysis software could then be exploited to detect and quantify these eDNA structures. Due to differences in pixel density between the background of the image and eDNA matrices, our software was able to detect and subsequently highlight eDNA structures. Comparison of automated eDNA detection versus manual detection rate confirmed a relatively high level of accuracy, with a non-detection rate of <8% (Fig. 3). Non-detected fragments were <5 μm and predicted to comprise colloidal particles and debris. To optimise accuracy, a minimum detection threshold of 5 μm was therefore set for subsequent analyses.

The software was designed to highlight eDNA structures with various colours to indicate different points of origin of each eDNA structure (Fig. 4). Information regarding their quantity and architecture could then be output. Specifically, data could be obtained regarding the total percentage of each field of view comprising eDNA, total eDNA stranding (μm/mm², total length of eDNA strands per mm²), average branch length (μm)

144 and average number of eDNA branches diverging from a single point (number of
145 junctions/number of branches per junction). To test this analysis capability, whilst
146 verifying the accuracy and sensitivity of this imaging approach in detecting eDNA,
147 studies were repeated in the presence of an increasing concentration (10–25 μg/ml) of
148 DNase I. As was anticipated, a significant reduction in eDNA levels was seen for both
149 DNase I concentrations tested (Fig. 5A). This was reflected in the quantification, as %
150 field of view comprising eDNA networks (Fig. 5B) and total eDNA stranding (Fig. 5C)
151 were significantly diminished following DNase I application. Variations in eDNA
152 architecture could also be measured. The average number of eDNA branches reduced
153 with increasing DNase I concentration (Fig. 5F), likely correlated with the general
154 reduction in eDNA levels, but no significant effect on average branch length (Fig. 5D) or
155 eDNA junction structure (Fig. 5E,G) was seen. DNase I had no significant impact on
156 overall biofilm biomass levels (Fig. S1). As a comparison with the time-dependent
157 differences in eDNA shown in Fig. 1, the imaging tool was also applied to analysis of 5 h
158 versus 24 h biofilms (Fig. S2). No significant differences in eDNA architecture were
159 observed, but eDNA levels were significantly diminished at 24 h compared to 5 h,
160 correlating with the soluble eDNA data. To explore if the differences in eDNA levels
161 were linked to time-dependent changes in nuclease activity, fluorescence-based DNase
162 activity assays were performed on cell bound- and secreted biofilm fractions (Fig. S3).
163 However, DNase activity was significantly lower at 24 h compared to 5 h. Together,
164 these data provided confidence that the imaging system could accurately detect eDNA
165 networks within biofilms and provide information relating to both quantities of eDNA and
166 the overall architecture of the eDNA networks. These data also implied that DNase I

could drive the removal and/or release of eDNA, thus reducing bulk quantity, but did not significantly impact its fundamental organisation.

Effects of carbon source on eDNA networks

Having confirmed the capacity for the imaging system to reliably detect and analyse eDNA networks, the next step was to exploit this approach to gain an improved understanding of eDNA within *S. gordonii* biofilms. For this work, a series of parameters were selected that had previously been implicated in modulating eDNA. The first of these was the effect of sugars. Prior studies had identified carbon catabolite dependent modulation of eDNA release in *S. gordonii* and *S. sanguinis* biofilms (34-36), and sucrose has been shown to promote eDNA dependent *S. mutans* biofilm formation, in which glucans were proposed to stabilise the eDNA matrices (37), (38). To validate whether the same trend could be observed within *S. gordonii* biofilms, our imaging system was exploited to examine the differential effects of glucose and sucrose on *S. gordonii* total eDNA stranding levels (Fig. 6A). Levels of eDNA for biofilms cultured in sucrose were 69% higher than those observed for glucose-cultured biofilms (Fig. 6B), while biomass levels differed by only 13% (Fig. 6G). No difference in eDNA architecture was observed (Fig. 6C-F). Furthermore, levels of eDNA in glucose-grown biofilms were unaffected by dextranase, although there was a 25% reduction in biomass (Fig. 6B,G). By contrast, a 76% decrease in eDNA levels was observed for the sucrose-grown biofilms following dextranase application, alongside a 25% reduction in biomass (Fig. 6B,G). Dextranase had no impact on eDNA branch length (Fig. 6C,D), but reductions were seen in numbers of junctions/branches per eDNA structure for both glucose- and

sucrose-grown biofilms (Fig. 6E,F). These data supported a role for glucans in eDNA networks within *S. gordonii* biofilms.

To further verify an association between eDNA levels and glucans, an *S. gordonii* Δ*gtfG* mutant was tested. Glucosyltransferase G (GtfG) is the only glucosyltransferase expressed by *S. gordonii,* is located extracellularly and is responsible for the generation of glucans during *S. gordonii* biofilm formation (39). GtfG hydrolyses dietary sucrose, synthesising glucose moieties into glucan polymers with α-1,6 and α-1,3 linkages (40, 41). In the presence of glucose, loss of GtfG reduced levels of eDNA by 53% but this effect was much more pronounced in the presence of sucrose, with a reduction of 84% (Fig. 7A,B). No effect was seen on biomass levels or eDNA branch length upon loss of GtfG with either condition (Fig. 7C-D,G) but as for dextranase, loss of GtfG resulted in reductions in numbers of junctions/branches per eDNA structure for sucrose-grown biofilms (Fig. 7E,F). Finally, to enable glucans to be visualised alongside eDNA, dextran conjugated to Alexa Fluor™ 647 was applied to the biofilms over the 5-h period. The fluorescently labelled dextran acts as an acceptor that is incorporated into newly formed glucans by Gtfs. As was expected, sucrose-cultured biofilms exhibited a significantly higher fluorescence output than their glucose-cultured counterparts, confirming a greater abundance of glucans (Fig. 8). Taken together, these data suggest a potential synergy between eDNA and glucans during *S. gordonii* biofilm formation, in which the glucans may serve to promote the structural stability of eDNA matrices.

Effects of DNase, SsnA, on eDNA networks

Application of exogenous nuclease enzymes has been shown to disrupt eDNA networks within biofilms (42, 43). Nuclease enzymes are also expressed by several bacterial species, but little is known about their capacity to modulate biofilm eDNA. Previous studies had identified the nuclease activity of *S. gordonii* and we have characterised this enzyme as Streptococcal Surface Nuclease A (SsnA) (44). We therefore generated a Δ*ssnA* mutant strain and utilised our imaging system to determine if SsnA can influence eDNA network formation during *S. gordonii* biofilm development. Levels of eDNA for Δ*ssnA* biofilms were 2.3-fold greater than those observed for *S. gordonii* WT biofilms (Fig. 9A), while total biomass levels (Fig. 9B) and eDNA architecture (Fig. S4) were comparable. This suggested that SsnA can influence *S. gordonii* eDNA levels and may have the capacity to manipulate or disperse eDNA networks as the biofilm develops. These studies were then extended to monitor the effects of SsnA in glucose or sucrose environments, since nuclease activity can be regulated by carbon catabolite availability (45, 46). Addition of glucose resulted in eDNA levels that were comparable to the Δ*ssnA* mutant in the absence of sugars and, as before, higher levels of eDNA were seen in the presence of sucrose. However, for both sugars, these effects were independent of SsnA, as no significant differences were seen for eDNA or biomass between the Δ*ssnA* mutant and *S. gordonii* WT (Fig. 9A,B). One potential explanation for this effect was that utilisation of the sugars via glycolysis and concomitant production of lactic acid, reduced the local pH to below the activity threshold for SsnA. To explore this, the pH of the culture media ± sugar supplementation following biofilm formation was measured. For

234 both glucose and sucrose, it was confirmed that pH levels fell below pH 7.0, which
235 would have significantly reduced SsnA activity (Table 3).
236
237 As a final assessment of the capacity for SsnA to modulate eDNA networks,
238 recombinant SsnA (rSsnA) was applied to biofilms formed by *S. gordonii* WT and Δ*ssnA*
239 strains (Fig. 9C,D). As before, no significant differences were seen in total biomass
240 levels between the two strains (Fig. 9D). By contrast, while exogenous SsnA had no
241 impact on the levels of eDNA for WT *S. gordonii* biofilms, the enhanced eDNA stranding
242 levels seen for Δ*ssnA* biofilms were reduced to WT levels following application of rSsnA
243 (Fig. 9C). Exogenous SsnA had no impact on overall eDNA architecture (Fig. S5) These
244 data provide further evidence of a role for SsnA in manipulating the eDNA networks of
245 *S. gordonii* biofilms under conditions permissive to enzymatic activity.
246
247 ***Modulation of eDNA networks via competence and Hpp systems***
248 A number of studies have implicated the competence (*comCDE*) system in regulating
249 eDNA release by *S. gordonii* (16-18, 47). We therefore used our imaging system to
250 verify the modulatory effects of the competence system on eDNA networks within *S.*
251 *gordonii* biofilms. A panel of knockout mutants defective in different stages of the
252 competence pathway were utilised for these studies: Δ*comC* (cannot express CSP),
253 Δ*comDE* (expresses but cannot detect CSP), Δ*comCDE* (cannot express or detect
254 CSP) and Δ*comR1/R2* (cannot upregulate competence genes in response to CSP).
255 Biomass levels were comparable for biofilms formed by all the strains tested (Fig. 10B).
256 By contrast, relative to WT, biofilms formed by strains Δ*comC*, Δ*comCDE* and

257 Δ*comR1/R2* exhibited significantly lower levels of eDNA, with reductions of 56%, 83%
258 and 68%, respectively (Fig. 10A). This confirmed the proposed role of competence
259 genes in mediating *S. gordonii* eDNA release and of CSP as the signal to induce these
260 effects. Unexpectedly, however, eDNA levels for Δ*comDE* biofilms were comparable to
261 those of WT, despite the absence of the cognate two-component signal system
262 (ComDE) to detect the CSP signal (Fig. 10A). This suggested that *S. gordonii* may be
263 utilising an alternative mechanism to detect CSP and this hypothesis was further
264 supported by complementation studies using exogenous CSP (Fig. 10C,D). As was
265 anticipated, application of exogenous CSP to Δ*comC* biofilms restored eDNA networks
266 to WT levels (Fig. 10C). No effect was seen for the already higher eDNA levels of WT
267 and Δ*comDE* biofilms. However, a significant (6-fold) increase was also seen in eDNA
268 following application of exogenous CSP to Δ*comCDE* biofilms, despite lacking the
269 ComDE CSP detection apparatus (Fig. 10C). Importantly, this response was specific to
270 CSP, as no such effect was seen following application of a scrambled CSP peptide as
271 control (data not shown). Assessment of eDNA architecture revealed some variation in
272 branch length or eDNA junction composition for the competence mutant biofilms relative
273 to WT (Fig. S6) but exogenous CSP had no significant effects (Fig. S7).
274
275 Another regulatory system that has been associated with competence in *S. gordonii* is
276 the hexa-heptapeptide permease (Hpp) system (48). The Hpp system is an oligopeptide
277 permease system comprising four constituents: HppA, HppB, HppG and HppH. HppA
278 has been implicated in substrate specific binding and along with HppH, transports
279 peptides comprising 5-7 amino acid residues across the cell envelope and into *S.*

gordonii cells. To ascertain whether the Hpp system may have capacity to detect CSP in the absence of ComDE and so facilitate CSP modulation of eDNA networks, knockout mutants lacking HppA or HppH, individually or in combination with Δ*comCDE*, were generated and tested. Slight variations were seen in biofilm biomass levels across the strains but the addition of exogenous CSP had no significant effects (Fig. 11A,C). By contrast, biofilms formed by mutants lacking HppA or HppH were reduced in eDNA levels relative to WT and these were restored upon application of exogenous CSP (Fig. 11A,B). For biofilms formed by strains lacking ComCDE in addition to HppA or HppH, levels of eDNA were significantly lower than those for WT biofilms but addition of exogenous CSP had no effect (Fig. 11A,B). It was also noted that the mutant lacking HppH formed biofilms that exhibited diminished numbers of branches/junctions per eDNA structure relative to WT (Fig. S8), suggesting that HppH (but not HppA) may contribute to eDNA architecture. Taken together, these data support the hypothesis that the Hpp system can engage CSP and that via CSP detection, both the ComCDE and Hpp systems can modulate eDNA networks within *S. gordonii* biofilms.

Discussion

Advances in fluorescence microscopy techniques have provided novel insights into the architecture of eDNA networks, showing them to form “web-” or “lattice-like” structures across the biofilm (9, 10). However, studies requiring the quantification of eDNA have had to rely on the analysis of soluble eDNA, which is disconnected from this complex eDNA architecture. To address this gap, this study presents use of a high-throughput image analysis tool that enables the visualisation and quantification of eDNA networks

303 *in situ* within biofilms. Furthermore, alongside quantification of eDNA abundance, this
304 imaging platform provides the ability to interrogate the detail of eDNA networks with
305 regards to, for example, eDNA branch length and number. Such high-level analysis of
306 eDNA architecture has not previously been possible.
307
308 To validate the capacity of this imaging system to both reliably detect eDNA and exhibit
309 sufficient sensitivity to detect differences in abundance, the effects of DNase I and
310 sugars were examined. As predicted, DNase I reduced total eDNA levels in a dose-
311 dependent manner. Nonetheless, some eDNA structures clearly remained following
312 DNase I application. These may represent Z-form eDNA, which accumulates as biofilms
313 mature and is recalcitrant to treatment with DNases (49). Additionally, as the biofilm
314 develops, eDNA matrices can be stabilised by DNA-binding proteins, which in turn may
315 limit access to eDNA structures by DNase enzymes (9, 12). In contrast to the effects of
316 DNase I, the presence of sucrose promoted eDNA production relative to glucose. This
317 correlates with the established role of H_2O_2 in regulating eDNA release by *S. gordonii*
318 (47, 50). H_2O_2 production is governed by SpxB, which in turn is under the control of
319 carbon catabolite regulator, CcpA (50). Moreover, these effects on eDNA directly
320 correlated with glucan production. The number of junctions within eDNA networks of
321 sucrose-grown biofilms were significantly diminished in the presence of dextranase or
322 the absence of GtfG. It is possible, therefore, that glucans may stabilise eDNA matrices
323 at points where eDNA branches, serving a similar role to DNA-binding proteins (9).This
324 correlates with studies using *S. mutans*, for which eDNA has also been shown to
325 increase in a glucan-dependent manner within biofilms (51-53). GtfB expressed by *S.*

mutans acts synergistically with eDNA to promote bacterial adherence to surfaces (54). With several *Streptococcus* species known to express Gtfs (55), glucan-mediated support of eDNA matrices may represent a common mechanism during biofilm development under conditions permissive to glucan production.

This study also demonstrated that surface associated nuclease SsnA of *S. gordonii* could modulate eDNA levels. SsnA has homology to SWAN of *S. sanguinis*, which has been shown to degrade neutrophil extracellular traps (20), but this is the first evidence of a surface-expressed nuclease influencing eDNA levels within biofilms. In the absence of SsnA, *S. gordonii* biofilms exhibited a greater abundance of eDNA networks, suggesting that SsnA may act directly on the eDNA strands to release or reorganise the networks. However, the impact of SsnA was significantly affected by conditions within the local environment. SsnA is primarily active in the pH range 7-10 (data not shown) and thus was rendered largely inactive in the presence of fermentable carbohydrate due to the resultant acidification of the environment from glycolysis. Nuclease enzyme expression has been observed from an array of oral biofilm commensals (44). As such, going forward, it will be interesting to determine the contribution that surface-bound nucleases make to organisation of the eDNA matrices found within polymicrobial biofilms of the oral cavity and at other sites, and the implications of variations in eDNA architecture for overall biofilm properties.

It has been recognised for some time that the competence (*comABCDE*) operon can regulate the release of eDNA by *S. gordonii* and *S. mutans* (4). During the competence

pathway in *S. gordonii*, pre-CSP (encoded by *comC*) is a 50 aa polypeptide that is cleaved by ComA to produce the mature 19 aa CSP. Mature CSP is transported out of the cell by the ComAB ABC binding cassette transporter and detected by two-component system (TCS) ComDE. ComD autophosphorylates upon detection of CSP and phosphorylates its intracellular response regulator, ComE. ComE subsequently modulates expression of the competence-specific alternative σ factor, ComR, which regulates transcription of the competence genes, including murein hydrolase LytF, enabling the bacterial cell to take up DNA from the environment (24, 47). Specific to eDNA release, it has been proposed that detection of CSP induces upregulation of AtlS that, in turn, upregulates expression SpxB. This results in an increase in the intracellular concentration of H_2O_2, with the resultant oxidative stress ultimately inducing LytF expression and eDNA release (4). The data presented in this study support the role of CSP in eDNA release. Specifically, our image analysis system revealed that the abundance of eDNA within *S. gordonii* biofilms was significantly diminished in the absence of CSP. Unexpectedly, however, it was also revealed that detection of CSP was not dependent on ComDE. Rather, the data imply that the Hpp system can serve as an alternative system for CSP detection and subsequent induction of downstream gene regulation. Cells lacking ComDE but with an intact Hpp system could respond to exogenous CSP, with a concomitant increase in eDNA abundance. Importantly, this was a specific effect, as no such elevation in eDNA levels was seen using a scrambled CSP peptide. Production of eDNA could not be rescued by the application of exogenous CSP to cells lacking both the ComDE and HppA/H detection apparatus, indicating that the cross-talk does not extend beyond these two systems.

As Hpp has been described as a hexa-heptapeptide permease system (48), it is yet to be understood how the 19 aa CSP can be detected. It is possible that some form of extracellular interaction causes signal transduction, without requiring full CSP entry to the cell. For example, for bacteria such as *Lactococcus lactis,* the Opp family proteins have been shown to detect peptides between 4-35 aa in length, as the whole peptide does not enter the recognition site of OppA (homologous to HppA in *S. gordonii*) (48, 56). Alternatively, CSP may be cleaved to a shorter length peptide prior to translocation into the cell via the Hpp system. In *S. mutans*, the 17 aa peptide ComS is processed at a double tryptophan motif (WW), releasing a 7 aa SigX inducing peptide (XIP) that is imported into the cell via an Opp system (57). As the mature *S. gordonii* CSP also possesses a WW motif, it is possible that this peptide may be processed in a similar way for recognition via the Hpp system. Exploring such possibilities will be the focus of future studies.

In summary, by exploiting our high-throughput image analysis tool, this study has provided a more detailed understanding of the factors that can modulate eDNA networks within *S. gordonii* biofilms. Evidence is provided of the capacity for glucans to stabilise eDNA matrices, while surface-bound nuclease SsnA has been shown to modify these structures under conditions permissive for enzymatic activity. Furthermore, while the role of CSP in inducing eDNA release is confirmed, a more complex regulatory mechanism has been revealed, with cross-talk with the Hpp system evident. Extending beyond *S. gordonii*, a critical feature of this imaging system is its capacity to

discriminate between eDNA strands, allowing a detailed quantification of the eDNA architecture *in situ* within biofilms that has not before been possible. In the studies presented here, it was possible to determine changes in eDNA branch length and junction composition and whilst current understanding is not yet sufficient to fully appreciate the biological implications of these modifications, there is clear potential for the high-level interrogation provided by this tool to help advance understanding of biofilm matrices. Going forward, it will be important to develop techniques that overcome or minimise current limitations relating to the need to detect Z-forms of eDNA, alongside B-form eDNA (49), and potential antibody accessibility issues (e.g. due to DNA-binding proteins or matrix accumulation), particularly for mature biofilms. Nonetheless, incorporation of this tool across the field of biofilm research offers the capacity to undertake a detailed assessment of how eDNA networks develop, how these networks contribute to the properties of the biofilm, and how this can be modulated. Such opportunities should significantly advance attempts to disrupt eDNA matrices within biofilms for therapeutic benefit, including oral biofilms.

Materials and Methods

Bacterial strains and growth conditions

Bacterial strains utilised in this study are listed in Table 1. *S. gordonii* wild-type and isogenic mutants were routinely cultured in Brain Heart Infusion broth (Lab Neogen) supplemented with 0.5% (w/v) yeast extract (BD; BHY) under stationary conditions for 16 h in a candle jar at 37^{o}C. As needed, broth cultures were supplemented with 100 µg/ml spectinomycin (Sp), 1.5 - 5 µg/ml erythromycin (Ery) or 250 µg/ml kanamycin

(Kan). A defined medium (YPT) was used for eDNA secretion studies comprising 20 mM NaH_2PO_4 (pH 7), 1 x yeast nitrogen base (Difco) and 0.1% (w/v) Bacto-tryptone ± supplementation with 0.2% (w/v) glucose or sucrose (19).

Mutagenesis of *S. gordonii*

Streptococcus gordonii DL1 (Challis) is predicted to express a 779-amino acid protein with 76% homology to streptococcal wall-anchored nuclease (SWAN), a nuclease in *Streptococcus sanguinis* capable of modulating the eDNA of neutrophil extracellular traps (20). The gene encoding this protein, designated streptococcal surface nuclease A (*ssnA*), was deleted by allelic exchange. In brief, flanking regions of *ssnA* were amplified by PCR using primer pairs SsnA.F1/R1 and SsnAF2/R2 (Table 2), while the *aad9* spectinomycin resistance cassette was amplified from plasmid pFW5 using SsnA.aad9F/R (Table 2)(21). Amplicons were joined by overlapping PCR using primers SsnA.F1/R2 (Table 2), yielding a final amplicon of 1936 bp. This was transformed into wild-type *S. gordonii* and successful mutagenesis confirmed by sequencing.

A similar allelic exchange approach was used to generate a Δ*comDE* mutant using primer pairs ComCD.F1/ComDE.R1 and ComDE.F1/ComCDE.R2 to amplify the upstream (884 bp) and downstream (619 bp) flanking regions, respectively, and primers Aad9.F/Aad9.R to amplify *aad9* from pFW5 (Table 2). Likewise, a Δ*comR1*/*R2* mutant was generated using primer pairs ComR1.F1/R1 with ComR1.F2/R2 or ComR2.F1/R1 with ComR2.F2/R2 to amplify the flanking regions of *comR1* or *comR2*, respectively (Table 2). These were joined to the *aad9* cassette from pFW5 (21) or the *ermAM* erythromycin resistance cassette from plasmid pVA838 (22) using primers

441 aad.ComR1.F/aad.ComR1.R or ermAM.ComR2.F/ermAM.ComR2.R, respectively
442 (Table 2). The *hppA* gene was inactivated by allelic exchange with *ermAM* using
443 primers hppA.F1/hppA.R1, hppA.F2/hppA.R2 and ermAM.hppAF/ermAM.hppAR (Table
444 2). The *hppH* gene was inactivated by allelic exchange with the *aphA3* kanamycin
445 resistance cassette from plasmid pDL276 (23) using primers hppH.F1/hppH.R1,
446 hppH.F2/hppH.R2 and aphA3.hppH.F/aphA3.hppH.R (Table 2). Final amplicons were
447 transformed into wild-type *S. gordonii*. Those for *hppA* and *hppH* were additionally
448 transformed into *S. gordonii* Δ*comCDE* (24).
449
450 ***Preparation of saliva***
451 Unstimulated whole saliva was collected on ice and pooled from a minimum of 5 healthy
452 adult donors who provided written consent (approved by the National Research Ethics
453 Committee Central Oxford C;08/H606/87). Pooled saliva was treated with 2.5 mM
454 dithiothreitol (DTT), incubated on ice for 10 min and centrifuged at 10,000 *g* for 10 min
455 to sediment mucins and bacteria. The supernatant was transferred to sterile
456 plasticware, diluted to 10% with distilled water and sterilised through a 0.45 μm filter.
457 Saliva-coated plates were assessed for DNase activity and the levels found to be
458 negligible (Fig. S9).
459
460 ***Biofilm formation***
461 Black, clear bottom 24-well plates (Sensoplate™, Greiner Bio-one) were incubated with
462 10% saliva (500 μl) for 16 h at 4^{o}C. Overnight broth cultures of *S. gordonii* were
463 harvested (5000 *g*, 7 min) and resuspended to OD_{600} 0.25 in YPT-glucose (YPTG;

equivalent to approximately 2.5x10⁶ CFU/ml). Saliva was aspirated from the plates, wells inoculated with 500 µl bacterial suspension and plates incubated in a humid environment at 37°C under gentle agitation (50 rpm) for up to 24 h. Following incubation, non-adherent cells were aspirated, the biofilms washed twice with YPT and either fixed with 4% (w/v) paraformaldehyde (PFA) for 16 h at 4°C for microscopy or resuspended in PBS for alternative applications. For some studies, bacterial suspensions were treated with dextranase (10 µg/ml; Sigma-Aldrich), DNase I (10-25 µg/ml, Sigma-Aldrich), or competence stimulating peptide (CSP, DVRSNKIRLWWENIFFNKK, 10 µg/ml; GenicBio) following inoculation of the plates. To measure glucan levels within the biofilm, dextran Alexa Fluor™ 647 conjugated antibody (1 µM, ThermoFisher Scientific) was applied alongside the bacterial suspension. Following incubation (5 h), wells were washed twice with YPT and fluorescence levels (ex/em: 650/668) measured with a plate reader (Infinite F200 Pro, Tecan). For assessment of biomass, biofilms were stained with 0.5% (w/v) crystal violet, washed with PBS to remove excess stain, and then biomass quantified by release of stain using 10% (v/v) glacial acetic acid and measurement of absorbance at A_{595}.

Soluble eDNA extraction and quantification

Biofilms from quadruplicate wells were collected into PBS and the soluble fraction recovered following centrifugation. Fractions were treated at 37 °C for 1 h with proteinase K (5 µg/ml; Sigma-Aldrich) and then the eDNA extracted using phenol:chloroform:isoamyl alcohol (25:24:1). The aqueous phase was collected, mixed with 3 M sodium acetate and isopropanol, and incubated for 1 h at 20°C. DNA was

precipitated and resuspended in dH_2O. DNA concentration and quality was then assessed by measurement at A_{260}/A_{280}.

High-throughput eDNA image capture and analysis

Following PFA fixation of biofilms, 2% (w/v) bovine serum albumin (Sigma-Aldrich), mouse anti-dsDNA antibody (ab27156, Abcam, 1:1000) and AlexaFluor-594®-conjugated secondary antibody (1:1000) were applied sequentially for 45 mins each. When required, *S. gordonii* cells were additionally stained with TO-PRO-3 (1:1000 dilution; ThermoFisher Scientific) for 15 min. A 20x magnification lens (HC PL APO 20x/0.75 CS2) on a Widefield Leica DMi600 microscope (Leica) coupled to a Photometrics Prime 95B cMOS camera (1200x1200, 11µm pixels, 8 bit, Photometrics) was employed to capture eDNA images using Leica acquisition software (LASX, Leica). eDNA structures were visualised using a cube consisting of a 560/40 nm excitation filter, 595 nm LP dichroic and 645/76 nm emission filter at an exposure time of up to 100 ms. Positions within each well were defined automatically using a custom-made MATLAB (Mathworks) programme which generated xyz positions to be used within the 'mark and find' function of LASX, facilitating the acquisition of at least 6 images per well. Each image covered an area of 660 x 660 µm and all images were taken in the same position in each well. All images were acquired as 10 µm Z-stacks (13 slices x 0.8 µm steps) to ensure images of eDNA at the optimum focus level were taken. Glucans within biofilm were visualised in a similar manner using a cube consisting of a 620/60 nm excitation filter, 660 nm LP dichroic and 700/38 nm emission filter.

Quantification of eDNA networks was performed using the Wolfson Bioimaging Facility modular image analysis Fiji plugin, MIA (25-27). Initially, eDNA was segmented from fluorescence images using 2D ridge detection (28, 29). Small gaps between proximal eDNA ends were then bridged, subject to user-defined alignment filters (end-end distance and maximum angular difference). Finally, length and branching metrics for the eDNA structures were obtained using the Analyze Skeleton plugin (30). Structural composition and abundance of eDNA were then assessed using Excel software (Microsoft).

Statistical analyses

Data were processed utilising Excel software (Microsoft) and analyses were performed using Prism (GraphPad Software, California, US). All experiments were performed at least in triplicate, unless otherwise stated, and data were analysed using Student's *t*-test (when comparing two groups) or general linear model (GLM) followed by one-way ANOVA and Tukey test (when comparing three or more groups).

Data availability

All experimental data associated with this work are openly available at the University of Bristol data repository, data.bris, at DOI: 10.5523/bris.2ottnygftntqz2ceivj35gx9ky. The modular image analysis macro is available at DOI: 10.5281/zenodo.3401275. The 2D ridge detection macro is available at DOI: 10.5281/zenodo.845874.

Acknowledgements

This work was funded by The Dunhill Medical Trust (RPGF1810\101). We acknowledge support from the Wolfson Bioimaging Facility and BrisSynBio, a BBSRC/EPSRC-funded Synthetic Biology Research Centre (grant number BB/L01386X/1). The authors declare no potential conflicts of interest with respect to the authorship and/or publication of this article.

References

1. Jakubovics NS, Grant Burgess J. Extracellular DNA in oral microbial biofilms. Microbes and Infection. 2015;17(7):531-7.
2. Nagler M, Insam H, Pietramellara G, Ascher-Jenull J. Extracellular DNA in natural environments: features, relevance and applications. Applied Microbiology and Biotechnology. 2018;102(15):6343-56.
3. Dadon Z, Cohen A, Szterenlicht YM, Assous MV, Barzilay Y, Raveh-Brawer D, et al. Spondylodiskitis and endocarditis due to *Streptococcus gordonii*. Ann Clin Microbiol Antimicrob. 2017;16(1):68.
4. Serrage HJ, Jepson MA, Rostami N, Jakubovics NS, Nobbs AH. Understanding the Matrix: The Role of Extracellular DNA in Oral Biofilms. Frontiers in Oral Health. 2021;2(7).
5. Jamal M, Ahmad W, Andleeb S, Jalil F, Imran M, Nawaz MA, et al. Bacterial biofilm and associated infections. J Chin Med Assoc. 2018;81(1):7-11.
6. Dengler V, Foulston L, DeFrancesco AS, Losick R. An electrostatic net model for the role of extracellular DNA in biofilm formation by *Staphylococcus aureus*. Journal of Bacteriology. 2015;197(24):3779-87.

7. Kavanaugh JS, Flack CE, Lister J, Ricker EB, Ibberson CB, Jenul C, et al. Identification of Extracellular DNA-Binding Proteins in the Biofilm Matrix. mBio. 2019;10(3).
8. Seviour T, Winnerdy FR, Wong LL, Shi X, Mugunthan S, Foo YH, et al. The biofilm matrix scaffold of *Pseudomonas aeruginosa* contains G-quadruplex extracellular DNA structures. npj Biofilms and Microbiomes. 2021;7(1):27.
9. Devaraj A, Buzzo JR, Mashburn-Warren L, Gloag ES, Novotny LA, Stoodley P, et al. The extracellular DNA lattice of bacterial biofilms is structurally related to Holliday junction recombination intermediates. Proceedings of the National Academy of Sciences. 2019;116(50):25068.
10. Barnes AMT, Ballering KS, Leibman RS, Wells CL, Dunnya GM. *Enterococcus faecalis* produces abundant extracellular structures containing DNA in the absence of cell lysis during early biofilm formation. mBio. 2012;3(4).
11. Devaraj A, Justice SS, Bakaletz LO, Goodman SD. DNABII proteins play a central role in UPEC biofilm structure. Molecular Microbiology. 2015;96(6):1119-35.
12. Devaraj A, Buzzo J, Rocco CJ, Bakaletz LO, Goodman SD. The DNABII family of proteins is comprised of the only nucleoid associated proteins required for nontypeable Haemophilus influenzae biofilm structure. MicrobiologyOpen. 2018;7(3).
13. Rocco CJ, Bakaletz LO, Goodman SD. Targeting the HUβ protein prevents *Porphyromonas gingivalis* from entering into preexisting biofilms. Journal of Bacteriology. 2018;200(11).

14. Rocco CJ, Davey ME, Bakaletz LO, Goodman SD. Natural antigenic differences in the functionally equivalent extracellular DNABII proteins of bacterial biofilms provide a means for targeted biofilm therapeutics. Molecular Oral Microbiology. 2017;32(2):118-30.
15. Loo CY, Corliss DA, Ganeshkumar N. *Streptococcus gordonii* biofilm formation: identification of genes that code for biofilm phenotypes. Journal of Bacteriology. 2000;182(5):1374-82.
16. Kreth J, Vu H, Zhang Y, Herzberg MC. Characterization of hydrogen peroxide-induced DNA release by *Streptococcus sanguinis* and *Streptococcus gordonii*. Journal of Bacteriology. 2009;191(20):6281-91.
17. Xu Y, Kreth J. Role of LytF and AtlS in eDNA Release by *Streptococcus gordonii*. PLoS ONE. 2013;8(4).
18. Itzek A, Zheng L, Chen Z, Merritt J, Kreth J. Hydrogen peroxide-dependent DNA release and transfer of antibiotic resistance genes in *Streptococcus gordonii*. Journal of Bacteriology. 2011;193(24):6912-22.
19. Dutton LC, Nobbs AH, Jepson K, Jepson MA, Vickerman MM, Aqeel Alawfi S, et al. *O*-mannosylation in *Candida albicans* enables development of interkingdom biofilm communities. mBio. 2014;5(2):e00911-e.
20. Morita C, Sumioka R, Nakata M, Okahashi N, Wada S, Yamashiro T, et al. Cell Wall-Anchored Nuclease of *Streptococcus sanguinis* Contributes to Escape from Neutrophil Extracellular Trap-Mediated Bacteriocidal Activity. PLOS ONE. 2014;9(8):e103125.

21. Podbielski A, Spellerberg B, Woischnik M, Pohl B, Lütticken R. Novel series of plasmid vectors for gene inactivation and expression analysis in group A streptococci (GAS). Gene. 1996;177(1-2):137-47.
22. Shimell MJ, Smith CJ, Tally FP, Macrina FL, Malamy MH. Hybridization studies reveal homologies between pBF4 and pBFTM10, Two clindamycin-erythromycin resistance transfer plasmids of *Bacteroides fragilis*. Journal of Bacteriology. 1982;152(2):950-3.
23. Dunny GM, Lee LN, LeBlanc DJ. Improved electroporation and cloning vector system for Gram-positive bacteria. Applied and Environmental Microbiology. 1991;57(4):1194-201.
24. Jack AA, Daniels DE, Jepson MA, Margaret Vickerman M, Lamont RJ, Jenkinson HF, et al. *Streptococcus gordonii comCDE* (competence) operon modulates biofilm formation with *Candida albicans*. Microbiology. 2015;161(2):411-21.
25. Rueden CT, Schindelin J, Hiner MC, DeZonia BE, Walter AE, Arena ET, et al. ImageJ2: ImageJ for the next generation of scientific image data. BMC Bioinformatics. 2017;18(1):529.
26. Schindelin J, Arganda-Carreras I, Frise E, Kaynig V, Longair M, Pietzsch T, et al. Fiji: an open-source platform for biological-image analysis. Nature Methods. 2012;9(7):676-82.
27. Cross S. MIA: Version 0.11.2. Zenodo. 2019. doi: 10.5281/zenodo.3401275.
28. Steger C. An unbiased detector of curvilinear structures. IEEE Transactions on Pattern Analysis and Machine Intelligence. 1998;20(2):113-25.
29. Wagner T. Ridge Detection v1.4.0. Zenodo. 2017. doi: 10.5281/zenodo.845874.

30. Arganda-Carreras I, Fernández-González R, Muñoz-Barrutia A, Ortiz-De-Solorzano C. 3D reconstruction of histological sections: Application to mammary gland tissue. Microsc Res Tech. 2010;73(11):1019-29.
31. Jin Y, Guo Y, Zhan Q, Shang Y, Qu D, Yu F. Subinhibitory concentrations of mupirocin stimulate *Staphylococcus aureus* biofilm formation by upregulating *cidA*. Antimicrobial Agents and Chemotherapy. 2020;64(3).
32. Yuan Z, Dai Y, Ouyang P, Rehman T, Hussain S, Zhang T, et al. Thymol inhibits biofilm formation, eliminates pre- existing biofilms, and enhances clearance of methicillin-resistant *Staphylococcus aureus* (MRSA) in a mouse peritoneal implant infection model. Microorganisms. 2020;8(1).
33. Padmavathi AR, Periyasamy M, Pandian SK. Assessment of 2,4-Di-tert-butylphenol induced modifications in extracellular polymeric substances of *Serratia marcescens*. Bioresource Technology. 2015;188:185-9.
34. Zheng L, Chen Z, Itzek A, Ashby M, Kreth J. Catabolite control protein a controls hydrogen peroxide production and cell death in *Streptococcus sanguinis*. Journal of Bacteriology. 2011;193(2):516-26.
35. Gilmore KS, Srinivas P, Akins DR, Hatter KL, Gilmore MS. Growth, development, and gene expression in a persistent *Streptococcus gordonii* biofilm. Infection and Immunity. 2003;71(8):4759-66.
36. Zheng L, Itzek A, Chen Z, Kreth J. Environmental influences on competitive hydrogen peroxide production in *Streptococcus gordonii*. Applied and Environmental Microbiology. 2011;77(13):4318-28.

37. Li Y, Du Y, Ye J, Wang B, Liu Y. Effect of extracellular DNA on the formation of *Streptococcus mutans* biofilm under sucrose environment. Chinese Journal of Stomatology. 2016;51(2):81-6.
38. Kim M, Jeon J, Kim J. *Streptococcus mutans* extracellular DNA levels depend on the number of bacteria in a biofilm. Scientific Reports. 2018;8(1):13313.
39. Koo H, Xiao J, Klein MI, Jeon JG. Exopolysaccharides produced by *Streptococcus mutans* glucosyltransferases modulate the establishment of microcolonies within multispecies biofilms. Journal of Bacteriology. 2010;192(12):3024-32.
40. Vickerman MM, Jones GW, Clewell DB. Molecular analysis of representative *Streptococcus gordonii* Spp phase variants reveals no differences in the glucosyltransferase structural gene, *gtfG*. Oral Microbiol Immunol. 1997;12(2):82-90.
41. Vickerman MM, Minick PE. Genetic analysis of the *rgg-gtfG* junctional region and its role in *Streptococcus gordonii* glucosyltransferase activity. Infect Immun. 2002;70(4):1703-14.
42. Rostami N, Shields RC, Yassin SA, Hawkins AR, Bowen L, Luo TL, et al. A Critical Role for Extracellular DNA in Dental Plaque Formation. Journal of Dental Research. 2017;96(2):208-16.
43. Brown HL, Reuter M, Hanman K, Betts RP, Van Vliet AHM. Prevention of biofilm formation and removal of existing biofilms by extracellular DNAses of *Campylobacter jejuni*. PLoS ONE. 2015;10(3).

44. Palmer LJ, Chapple IL, Wright HJ, Roberts A, Cooper PR. Extracellular deoxyribonuclease production by periodontal bacteria. J Periodontal Res. 2012;47(4):439-45.
45. Doke M, Fukamachi H, Morisaki H, Arimoto T, Kataoka H, Kuwata H. Nucleases from *Prevotella intermedia* can degrade neutrophil extracellular traps. Molecular Oral Microbiology. 2017;32(4):288-300.
46. Kiedrowski MR, Kavanaugh JS, Malone CL, Mootz JM, Voyich JM, Smeltzer MS, et al. Nuclease Modulates Biofilm Formation in Community-Associated Methicillin-Resistant *Staphylococcus aureus*. PLOS ONE. 2011;6(11):e26714.
47. Zheng L, Chen Z, Itzek A, Herzberg MC, Kreth J. CcpA regulates biofilm formation and competence in *Streptococcus gordonii*. Molecular Oral Microbiology. 2012;27(2):83-94.
48. Jenkinson HF, Baker RA, Tannock GW. A binding-lipoprotein-dependent oligopeptide transport system in *Streptococcus gordonii* essential for uptake of hexa- and heptapeptides. Journal of Bacteriology. 1996;178(1):68-77.
49. Buzzo JR, Devaraj A, Gloag ES, Jurcisek JA, Robledo-Avila F, Kesler T, et al. Z-form extracellular DNA is a structural component of the bacterial biofilm matrix. Cell. 2021;184(23):5740-58.
50. Redanz S, Masilamani R, Cullin N, Giacaman RA, Merritt J, Kreth J. Distinct Regulatory Role of Carbon Catabolite Protein A (CcpA) in Oral Streptococcal Expression. Journal of Bacteriology. 2018;200(8):e00619-17.

51. Li Y, Du Y, Ye J, Wang B, Liu Y. Effect of extracellular DNA on the formation of *Streptococcus mutans* biofilm under sucrose environment. Chinese Journal of Stomatology. 2016;51(2):81-6.
52. Klein MI, DeBaz L, Agidi S, Lee H, Xie G, Lin AHM, et al. Dynamics of *Streptococcus mutans* Transcriptome in Response to Starch and Sucrose during Biofilm Development. PLOS ONE. 2010;5(10):e13478.
53. Nagasawa R, Sato T, Senpuku H. Raffinose induces biofilm formation by *Streptococcus mutans* in low concentrations of sucrose by increasing production of extracellular DNA and fructan. Applied and Environmental Microbiology. 2017;83(15).
54. Liao S, Klein MI, Heim KP, Fan Y, Bitoun JP, Ahn S-J, et al. *Streptococcus mutans* extracellular DNA is upregulated during growth in biofilms, actively released via membrane vesicles, and influenced by components of the protein secretion machinery. Journal of Bacteriology. 2014;196(13):2355-66.
55. Xu RR, Yang WD, Niu KX, Wang B, Wang WM. An update on the evolution of glucosyltransferase (*gtf*) genes in *Streptococcus*. Frontiers in Microbiology. 2018;9.
56. Lamarque M, Charbonnel P, Aubel D, Piard JC, Atlan D, Juillard V. A multifunction ABC transporter (Opt) contributes to diversity of peptide uptake specificity within the genus *Lactococcus*. J Bacteriol. 2004;186(19):6492-500.
57. Mashburn-Warren L, Morrison DA, Federle MJ. A novel double-tryptophan peptide pheromone controls competence in *Streptococcus* spp. via an Rgg regulator. Mol Microbiol. 2010;78(3):589-606.

58. Vickerman MM, Iobst S, Jesionowski AM, Gill SR. Genome-wide transcriptional changes in *Streptococcus gordonii* in response to competence signaling peptide. J Bacteriol. 2007;189(21):7799-807.

59. Vickerman MM, Wang M, Baker LJ. An amino acid change near the carboxyl terminus of the *Streptococcus gordonii* regulatory protein Rgg affects its abilities to bind DNA and influence expression of the glucosyltransferase gene *gtfG*. Microbiology. 2003;149:399-406.

719 **Table 1**: Strains used in this study

Identifier	Strain	Relevant Characteristics	Ref
UB1507	DL1 (Challis)	Parental Strain	(58)
UB653	Δ*gtfG*	*gtfG*::*aad9*	(59)
UB2660	Δ*comC*	*comC*::*aad9*	(24)
UB2661	Δ*comDE*	*comCD*::*aad9*	This study
UB2347	Δ*comCDE*	*comCDE*::*aad9*	(24)
UB2975	Δ*comR1R2*	*comR1::aad9 comR2::ermAM*	This study
UB2953	Δ*hppA*	*hppA::ermAM*	This study
UB2958	Δ*hppA* Δ*comCDE*	*hppA::ermAM comCDE*::*aad9*	This study
UB3097	Δ*hppH*	*hppH::aphA3*	This study
UB3098	Δ*hppH* Δ*comCDE*	*hppH::aphA3 comCDE*::*aad9*	This study
UB2886	Δ*ssnA*	*ssnA::aad9*	Rostami et al

720

721 **Table 2** Primers used in this study

Mutant generated	**Primer name**	**Primer sequence**	**Function**
Δ*ssnA*	*SsnA.F1*	TTTTATCAGAAATTGATTG	Amplify 484-bp amplicon upstream of *ssnA*
	SsnA.R1	AAAGTTCTCCTTTTCCTA	
	SsnA.F2	CCTAGAGTAAGCTCTAAACA	Amplify 674-bp amplicon downstream of *ssnA*
	SsnA.R2	TGTCAAAGCTACCAGTAC	
	aad9_SsnAF	AGGAGAACTTTATGAATACATAC GAACAAATTAATA	Amplify 782-bp *aad9* cassette from pFW5 with overlaps for *ssnA* flanking regions
	aad9_SsnAR	GCTTACTCTCTAGGTTATAATTT TTTTAATCTGTTATTTAA	
Δ*comDE*	*ComCD.F1*	CGACTCAGTCGTTTTACGAAAG GGAGATTGAAATGATATTTACAA TGGATCCGACAAAG	Amplify 448-bp amplicon upstream of *comDE*
	ComDE.R1		
	ComDE.F1	TTACAATGGATCCGACAAAGCG AGATAAACTGG	Amplify 619-bp amplicon downstream of
	ComCDE.R2	CTACTTCGCGGATATTGGC	

			comDE
	ComDE_Aad9F *ComDE_ Aad9R*	GGAGATATTTTTTTGAATACATA CGAACAAATT GTTAGAGGATTTTAATATTAAAA AAATTAGACAATAAAT	Amplify 1100-bp *aad9* cassette from pFW5 with overlaps for *comDE* flanking regions
∆*comR1*	*ComR1.F1* *ComR1.R1*	GATATTCCAGGATCCTGCTG TATGTATTCATTGACTAGTCCTT TCTTTTTG	Amplify 586-bp amplicon upstream of *comR1*
	ComR1.F2 *ComR1.R2*	AAAAAATTATAAAAAGAAGGGA GAGGCAATC CCTCAGCGTCAGTTACAGAC	Amplify 1075-bp amplicon downstream of *comR1*
	aad9.comr1F *aad.comR1R*	GACTAGTCAATGAATACATACG AACAAATTAATA CCTTCTTTTTATAATTTTTTTAAT CTGTTATTTAA	Amplify 770-bp *aad9* cassette from pFW5 with overlaps for *comR1* flanking regions
∆*comR2*	*ComR2.F1* *ComR2.R1*	TCCAGGTGCATATAATCCAC ATTTTTGTTCATTGACTAGTCCT TTCTTTTTG	Amplify 840-bp amplicon upstream of *comR2*

	ComR2.F2 *ComR2.R2*	GGAGGAAATAAAAAGAAGGGAG AGGCAATC CCTCAGCGTCAGTTACAGAC	Amplify 1075-bp amplicon upstream of *comR2*
	ermAM.comR2F *ermAM.comR2R*	ACTAGTCAATGAACAAAAATATA AAATATTCTCAAAAC CCCTTCTTTTTATTTCCTCCCGT TAAATAATAG	Amplify 755-bp *ermAM* cassette from pVA838 with overlaps for *comR2* flanking regions
∆*hppA*	*HppA.F1* *HppA.R1*	CAACAATCCAGACCAATACTC GAAATGGAGAATATACGATGAA CAAAAA	Amplify 953-bp amplicon upstream of *hppA.*
	HppA.F2 *HppA.R2*	CGGGAGGAAATAACCAATCATT AGAACTTTC CCATCCATGCTTGTTAGC	Amplify 932-bp amplicon downstream of *hppA*
	ermAM.hppAF *ermAM.hppAR*	AATATACGATGAACAAAAATATA AAATATTCTC TGATTGGTTATTTCCTCCCGTTA AATA	Amplify 753-bp *ermAM* cassette from pVA838 with overlaps for *comR2* flanking regions
∆*hppH*	*HppH.F1*	CCCGATTCACTTAGATCTTC	Amplify 901-bp

	HppH.R1	CATTTTAGCCATGAAATACTCCTTTCAAAATA	amplicon upstream of *hppH*
	HppH.F2 *HppH.R2*	ATTGTTTTAGCAATTACCCTAACGAGGAGG GATACTTGTCGGGTCAGTAGC	Amplify 906-bp amplicon upstream of *hppH.*
	aphA3.hppH F *aphA3.hppH R*	AGTATTTCATGGCTAAAATGAGAATATCACC AGGGTAATTGCTAAAACAATTCATCCAGTAAAATA	Amplify 813-bp *aphA3* cassette from pDL276 with overlaps for *comR2* flanking regions

722

723 **Table 3:** Media pH of 5 h biofilms

	Strain	pH*
Untreated	WT	7.11 ± 0.03
	WT + SsnA	7.18 ± 0.06
	ΔssnA	7.16 ± 0.11
	ΔssnA + SsnA	7.15 ± 0.11
0.2% Glucose	WT	6.85 ± 0.06
	ΔssnA	6.84 ± 0.10
0.2% Sucrose	WT	6.26 ± 0.09
	ΔssnA	6.66 ± 0.11

724 *Data is presented as mean ± SD, n = 8.

725

Figure 1. Changes in *S. gordonii* biofilm biomass and eDNA over time. WT *S. gordonii* biofilms were grown at 37 °C in YPTG on saliva-coated 24-well plates for up to 24 h and levels of biomass determined by crystal violet staining (line) or eDNA assessed using the phenol:chloroform:isoamyl DNA extraction method (columns). Data are presented as mean values ± SD. *P< 0.05, **P< 0.01 or ****P< 0.0001 compared to 1 h value as determined by one-way ANOVA followed by post-hoc Tukey Test (n=3).

Figure 2. Interwoven networks of eDNA in *S. gordonii* biofilm. WT *S. gordonii* biofilms were grown at 37°C in YPTG on saliva-coated 24-well plates for 5 h. Networks of eDNA (red) and *S. gordonii* biofilm cells (green) were fluorescently labelled and visualised by widefield microscopy. Representative images are shown. Scale bar, 50 µm.

Figure 3. Optimisation of automated eDNA detection. WT *S. gordonii* biofilms were grown at 37°C in YPTG on saliva-coated 24-well plates for 5 h. Networks of eDNA were then immunolabelled and visualised by widefield microscopy (A). Image analysis software was used to detect and quantify eDNA strands and reliability of this system was assessed (B). Different colours denote complete detection (green), fragmented detection (orange), undetected (magenta), non-eDNA (cyan) and background particles (white/not highlighted). Representative images are shown. Scale bars, 50 µm.

Figure 4. Visualization of eDNA in *S. gordonii* biofilms at 5 h. WT *S. gordonii* biofilms were grown at 37 °C in YPTG on saliva-coated 24-well plates for 5 h. Networks of eDNA were then immunolabelled and visualized by widefield microscopy (A). Image

analysis software was used to detect and quantify eDNA strands, as shown in (C). (B, D) correspond to higher resolution images of the section indicated by the red box in (A, C). Representative images are shown. Scale bars, 50 μm.

Figure 5. eDNA detection and quantification following DNase I treatment. WT *S. gordonii* biofilms were grown at 37 °C in YPTG ± 10-25 μg/ml DNase I on saliva-coated 24-well plates for 5 h. Networks of eDNA were then immunolabelled and visualized by widefield microscopy (A, i - iii) and image software used to detect eDNA networks (A, iv – vi). Quantifiable differences in the % of field of view comprising eDNA (B), total eDNA stranding per mm² (C), average eDNA branch length (D), average maximum eDNA branch length (E), average number of branches per field of view (F) and average number of junctions per eDNA structure (G) were then assessed using Excel. Data are presented as mean ± SD.**P<0.01, *P<0.05 relative to untreated (UT) control, as determined via one-way ANOVA followed by Tukey test (n = 3). Scale bars, 50 μm.

Figure 6. Glucans enhance eDNA levels within sucrose-grown biofilms. WT *S. gordonii* biofilms were grown on saliva-coated 24-well plates for 5 h at 37 °C in YPT ± 0.2% glucose/sucrose in the absence (UT) or presence of 10 μg/ml dextranase (Dex). eDNA stranding (A, B), eDNA branching (C, D), number of junctions/branches per eDNA structure (E, F) and levels of biomass (G) were then determined by microscopy or crystal violet staining, respectively. Data are presented as mean ± SD. *P<0.05 and **P<0.01, as determined via one-way ANOVA followed by Tukey test (n = 3).

Figure 7. Inability to synthesise glucans impairs eDNA levels within biofilms. WT and Δ*gtfG S. gordonii* biofilms were grown for 5 h at 37 °C in YPT ± 0.2% glucose/sucrose. eDNA stranding was assessed via widefield microscopy (A) and quantified (B-F). Levels of biomass (G) were determined by crystal violet staining. Data are presented as mean ± SD. *P<0.05, **P<0.01 and ***P<0.001, as determined via one-way ANOVA followed by Tukey test (n = 3). Representative images are shown. Scale bars, 50 μm.

Figure 8. Sucrose elevates glucan levels within *S. gordonii* biofilms. WT *S. gordonii* biofilms were grown on saliva-coated 24-well plates for 5 h at 37 °C in YPT ± 0.2% glucose/sucrose. Relative levels of glucans were measured by inclusion of Alexa Fluor™ 647 conjugated dextran during biofilm development and subsequent quantification of fluorescence levels. Data are presented as mean ± SD. *P<0.05, as determined via Student's t-test (n = 3).

Figure 9. SsnA can modulate eDNA levels but is affected by carbon source. *S. gordonii* WT and Δ*ssnA* biofilms were grown on saliva-coated 24-well plates for 5 h at 37 °C in YPT in the absence (UT) or presence of 0.2% glucose/sucrose. eDNA stranding (A) and levels of biomass (B) were determined by microscopy or crystal violet staining, respectively. *S. gordonii* WT and Δ*ssnA* biofilms were also grown ± 5 μg/ml SsnA and eDNA stranding (C) and biomass (D) were determined as above. Data are presented as mean ± SD (n = 3). *P<0.05 and ***P<0.001, as determined via one-way ANOVA followed by Tukey test.

Figure 10. CSP modulates eDNA stranding in *S. gordonii* biofilms, even in absence of ComDE apparatus. WT *S. gordonii* and various *comCDE* operon mutant strains were grown at 37 °C in YPTG on saliva-coated 24-well plates in the absence (white bars) or presence (grey bars) of CSP for 5 h. Levels of eDNA stranding (A, C) and biomass (B, D) and were then determined by microscopy or crystal violet staining, respectively. Data are presented as mean ± SD (n = 3; Δ*comDE*, n = 2). *P< 0.05, **P<0.01, ***P<0.001 or **** P< 0.0001, as determined by one way ANOVA followed by Tukey test.

Figure 11. Hpp system responds to CSP to modulate eDNA. WT S. *gordonii* or *hpp* ± *comCDE* system mutants were grown at 37 °C in YPTG on saliva-coated 24-well plates ± 10 µg/ml CSP for 5 h. Levels of eDNA stranding (A,B) and biomass (C) were then determined by microscopy or crystal violet staining, respectively. (A) indicates representative images of eDNA stranding. Data are presented as mean ± SD. *P<0.05 or **P<0.01, as determined by two-way ANOVA followed by Tukey test; n = 3/4. Scale bars, 50 µm.

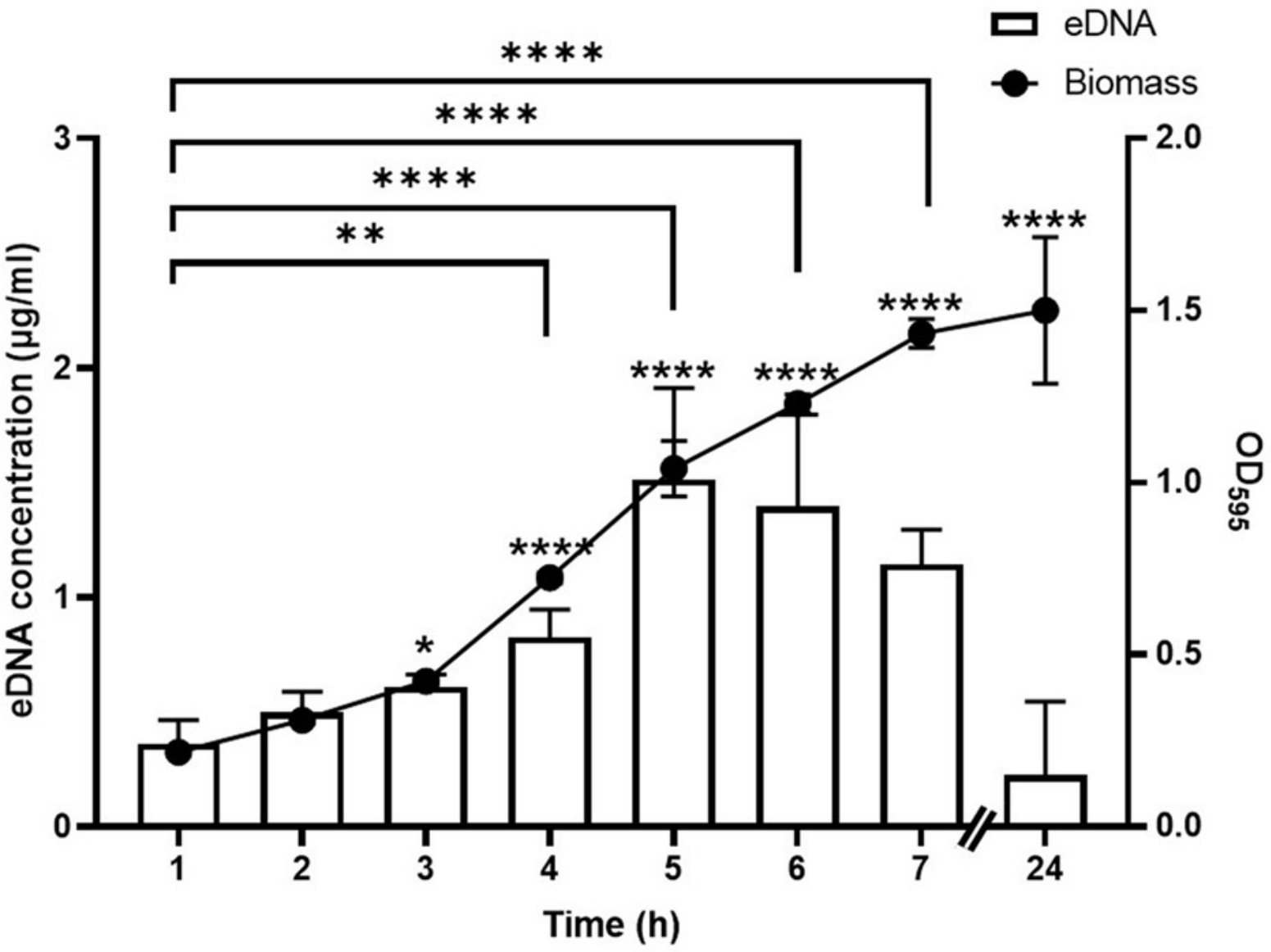
eDNA
Biomass
****
****
****
**
****
****
****
****
*
eDNA concentration (µg/ml)
OD595
Time (h)
0
1
2
3
0.0
0.5
1.0
1.5
2.0
1
2
3
4
5
6
7
24

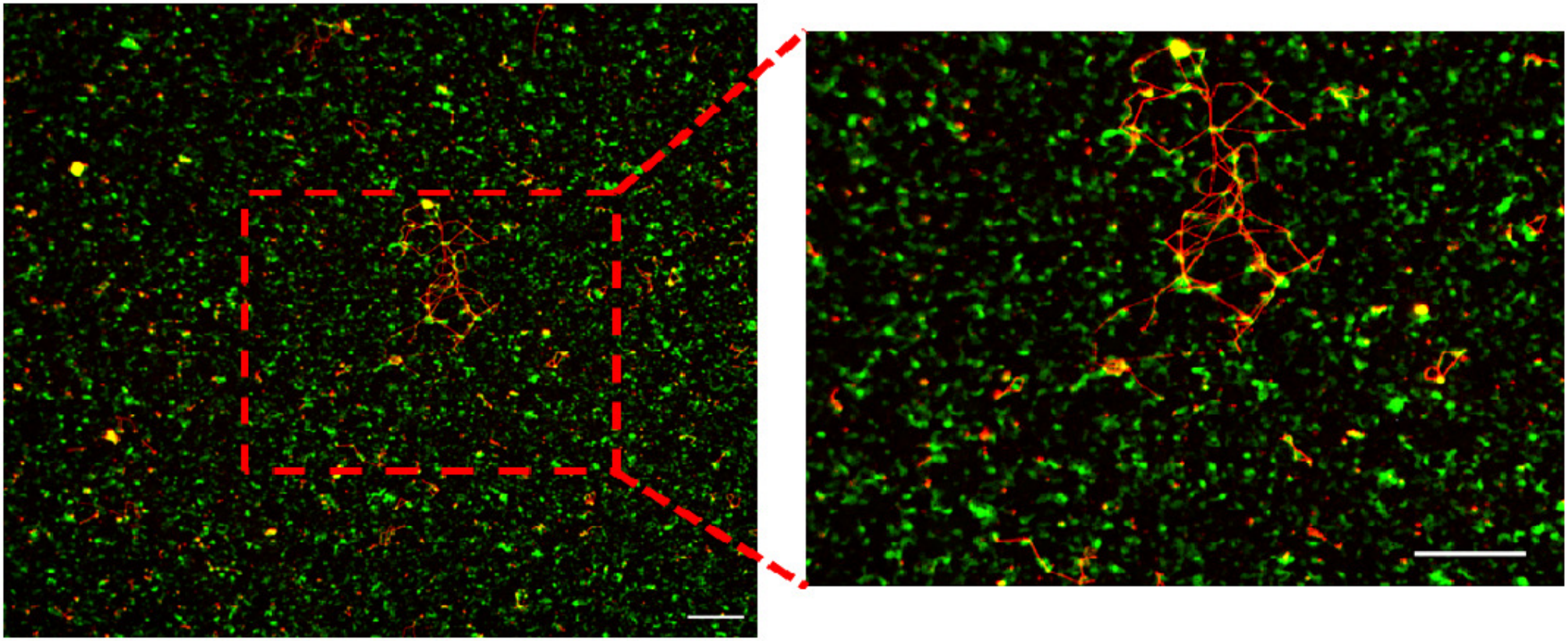

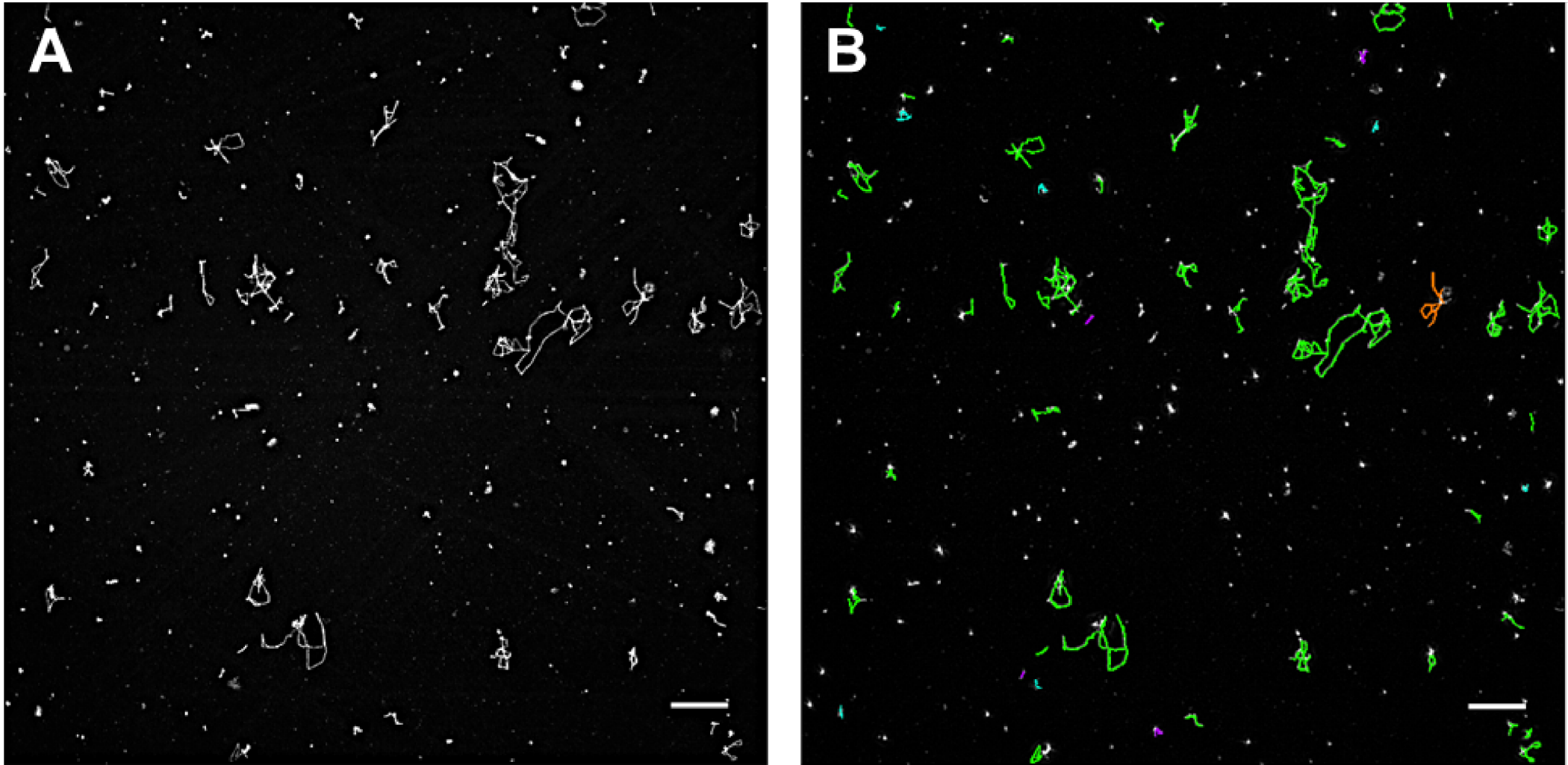
A
B

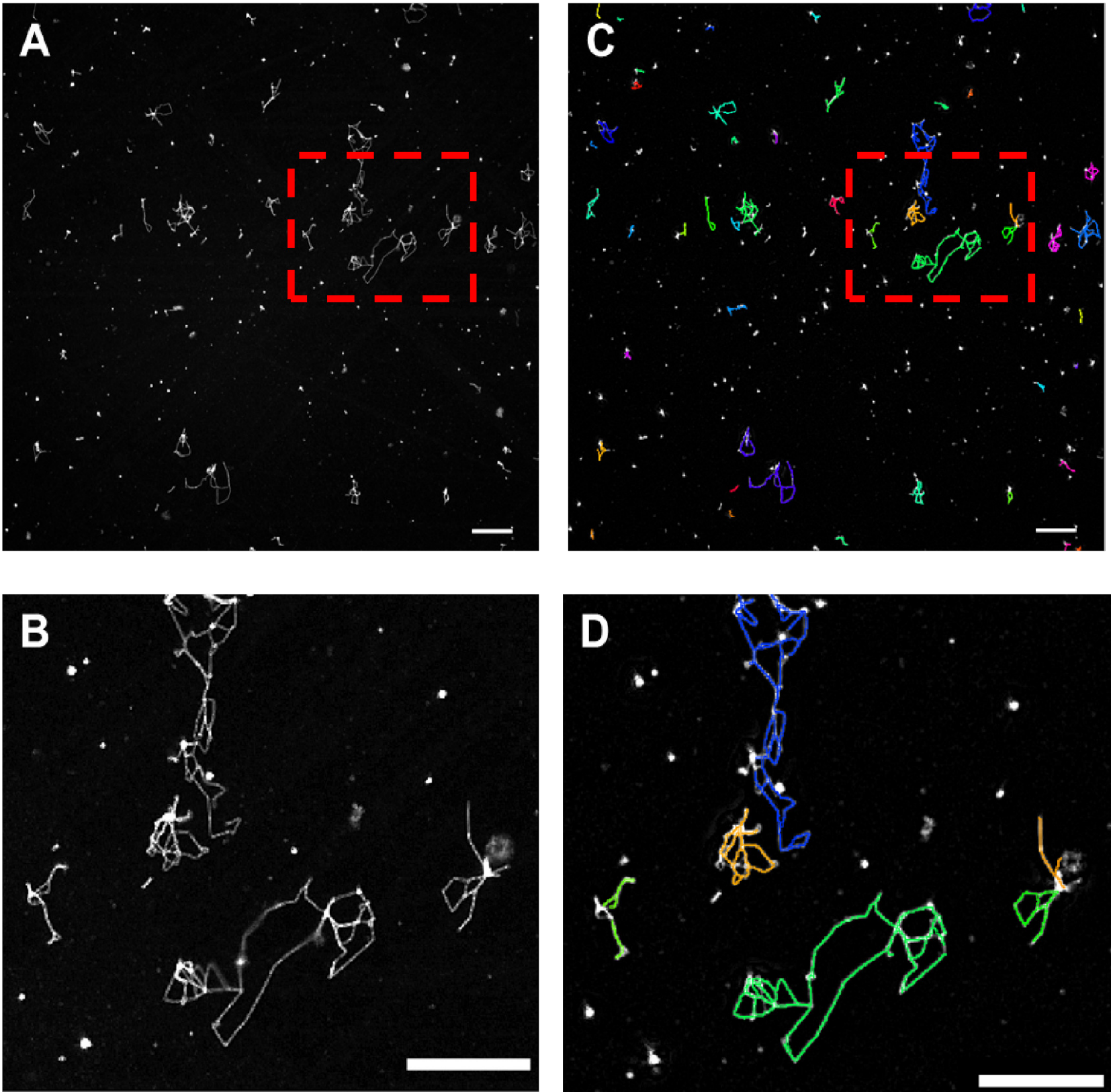
A
C
B
D

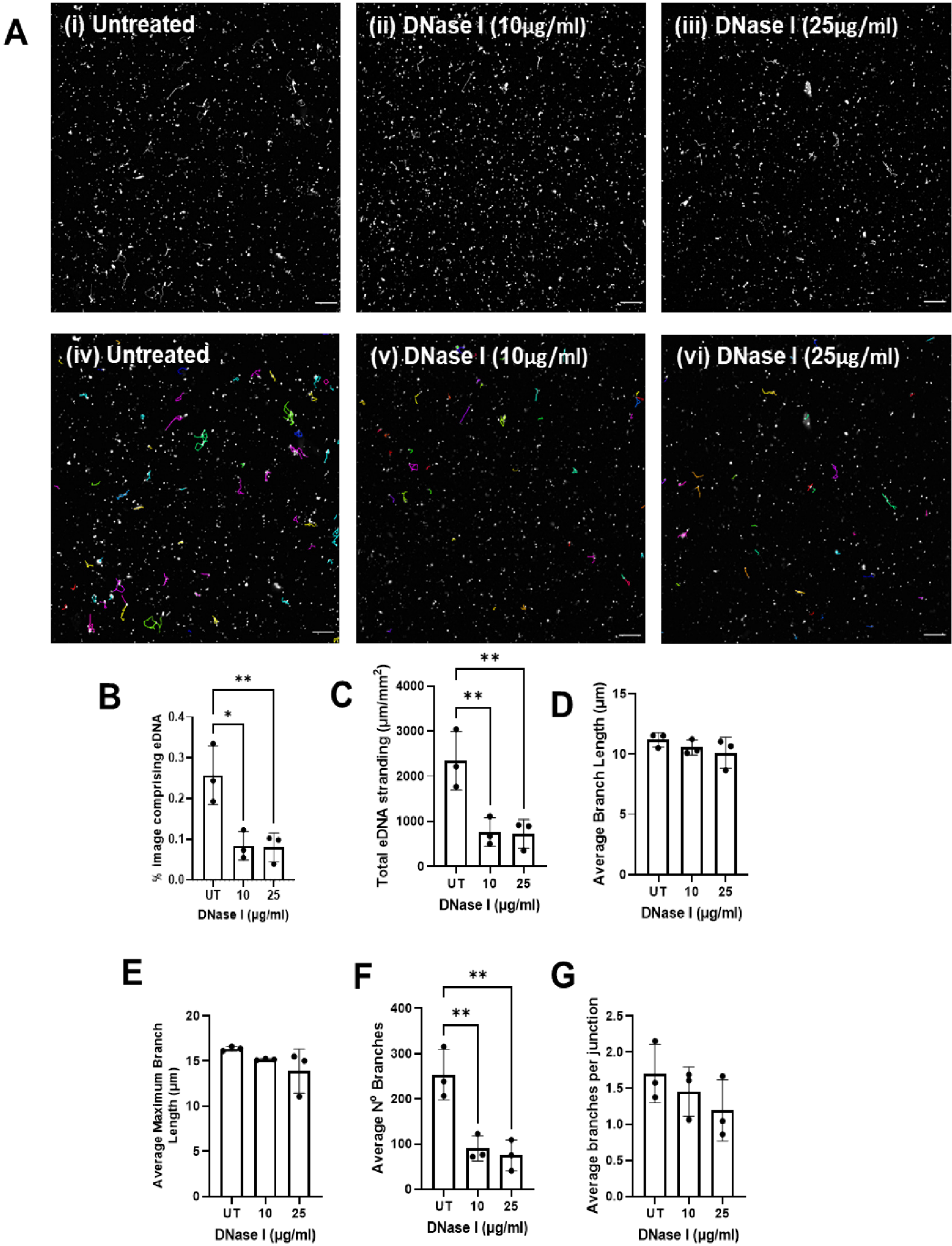
A
(i) Untreated
(ii) DNase I (10µg/ml)
(iii) DNase I (25µg/ml)
(iv) Untreated
(v) DNase I (10µg/ml)
(vi) DNase I (25µg/ml)
B
% Image comprising eDNA
0.0
0.1
0.2
0.3
0.4
*
**
UT
10
25
DNase I (µg/ml)
C
Total eDNA stranding (µm/mm²)
0
1000
2000
3000
4000
**
**
UT
10
25
DNase I (µg/ml)
D
Average Branch Length (µm)
0
5
10
15
UT
10
25
DNase I (µg/ml)
E
Average Maximum Branch Length (µm)
0
5
10
15
20
UT
10
25
DNase I (µg/ml)
F
Average N° Branches
0
100
200
300
400
**
**
UT
10
25
DNase I (µg/ml)
G
Average branches per junction
0.0
0.5
1.0
1.5
2.0
2.5
UT
10
25
DNase I (µg/ml)

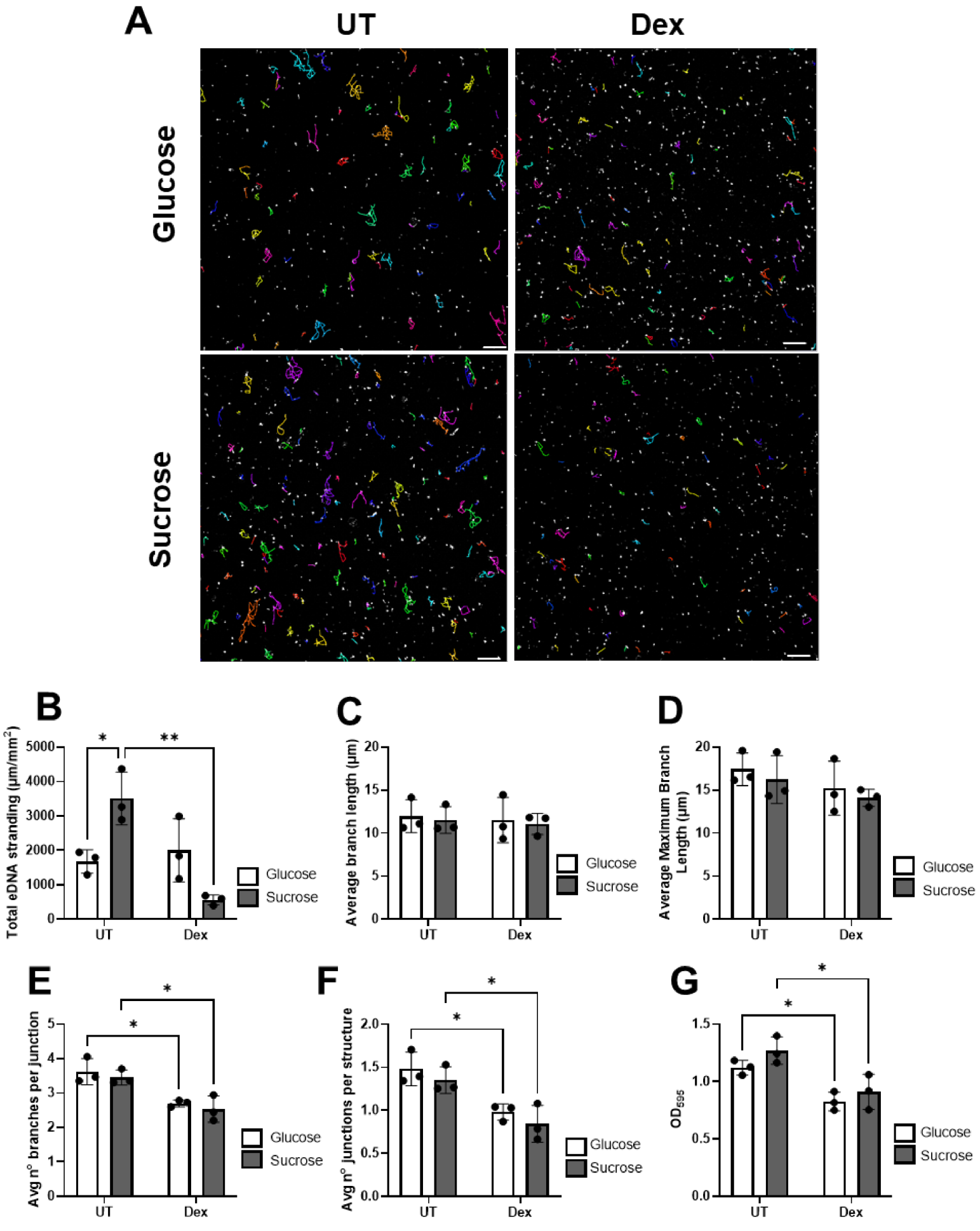
A
UT
Dex
Glucose
Sucrose
B
Total eDNA stranding (µm/mm²)
5000
4000
3000
2000
1000
0
*
**
UT
Dex
Glucose
Sucrose
C
Average branch length (µm)
20
15
10
5
0
UT
Dex
Glucose
Sucrose
D
Average Maximum Branch Length (µm)
20
15
10
5
0
UT
Dex
Glucose
Sucrose
E
Avg n° branches per junction
5
4
3
2
1
0
*
*
UT
Dex
Glucose
Sucrose
F
Avg n° junctions per structure
2.0
1.5
1.0
0.5
0.0
*
*
UT
Dex
Glucose
Sucrose
G
OD595
1.5
1.0
0.5
0.0
*
*
UT
Dex
Glucose
Sucrose

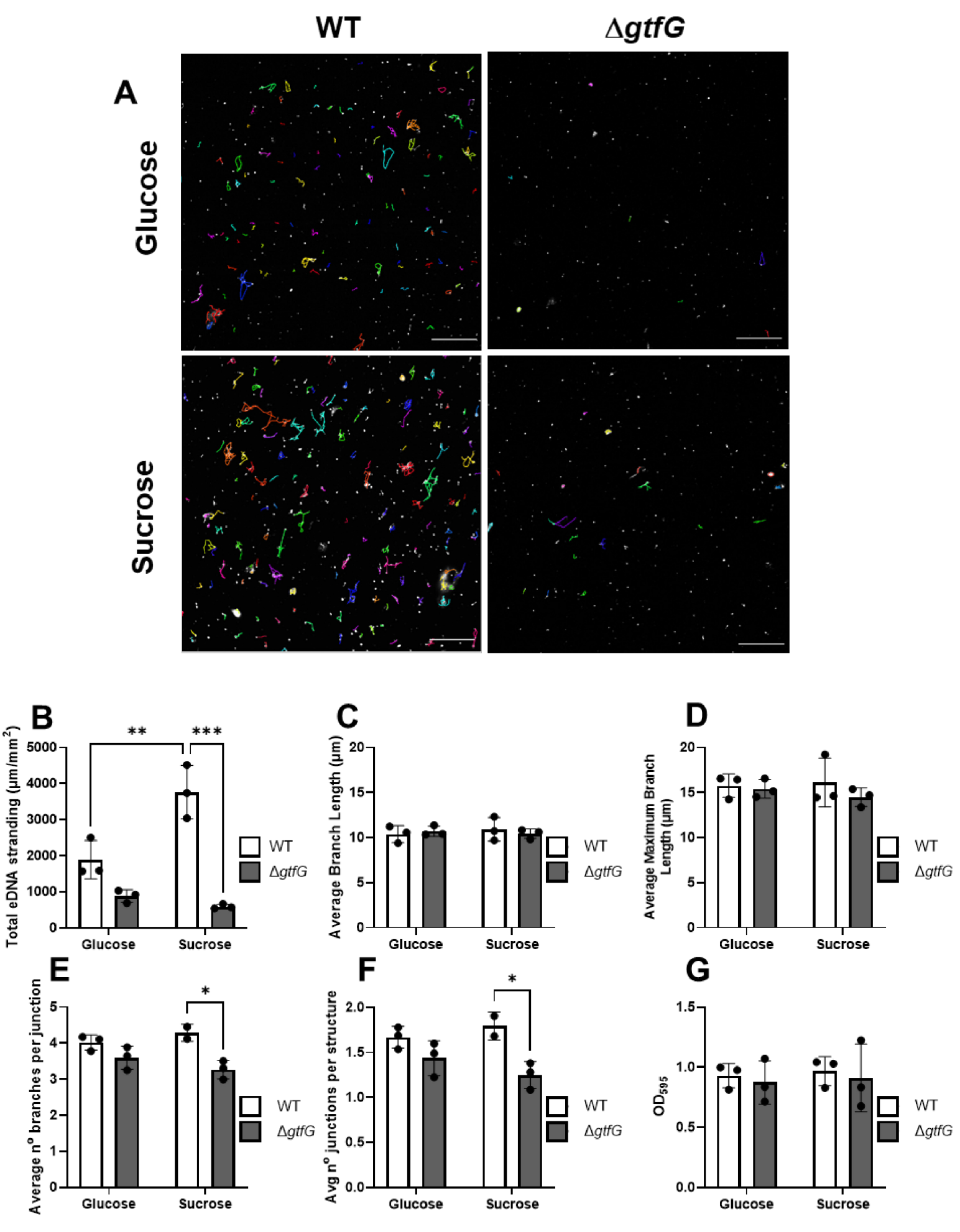
WT
ΔgtfG
A
Glucose
Sucrose
B
Total eDNA stranding (µm/mm²)
**
***
5000
4000
3000
2000
1000
0
Glucose
Sucrose
WT
ΔgtfG
C
Average Branch Length (µm)
20
15
10
5
0
Glucose
Sucrose
WT
ΔgtfG
D
Average Maximum Branch Length (µm)
20
15
10
5
0
Glucose
Sucrose
WT
ΔgtfG
E
Average n° branches per junction
*
5
4
3
2
1
0
Glucose
Sucrose
WT
ΔgtfG
F
Avg n° junctions per structure
*
2.0
1.5
1.0
0.5
0.0
Glucose
Sucrose
WT
ΔgtfG
G
OD595
1.5
1.0
0.5
0.0
Glucose
Sucrose
WT
ΔgtfG

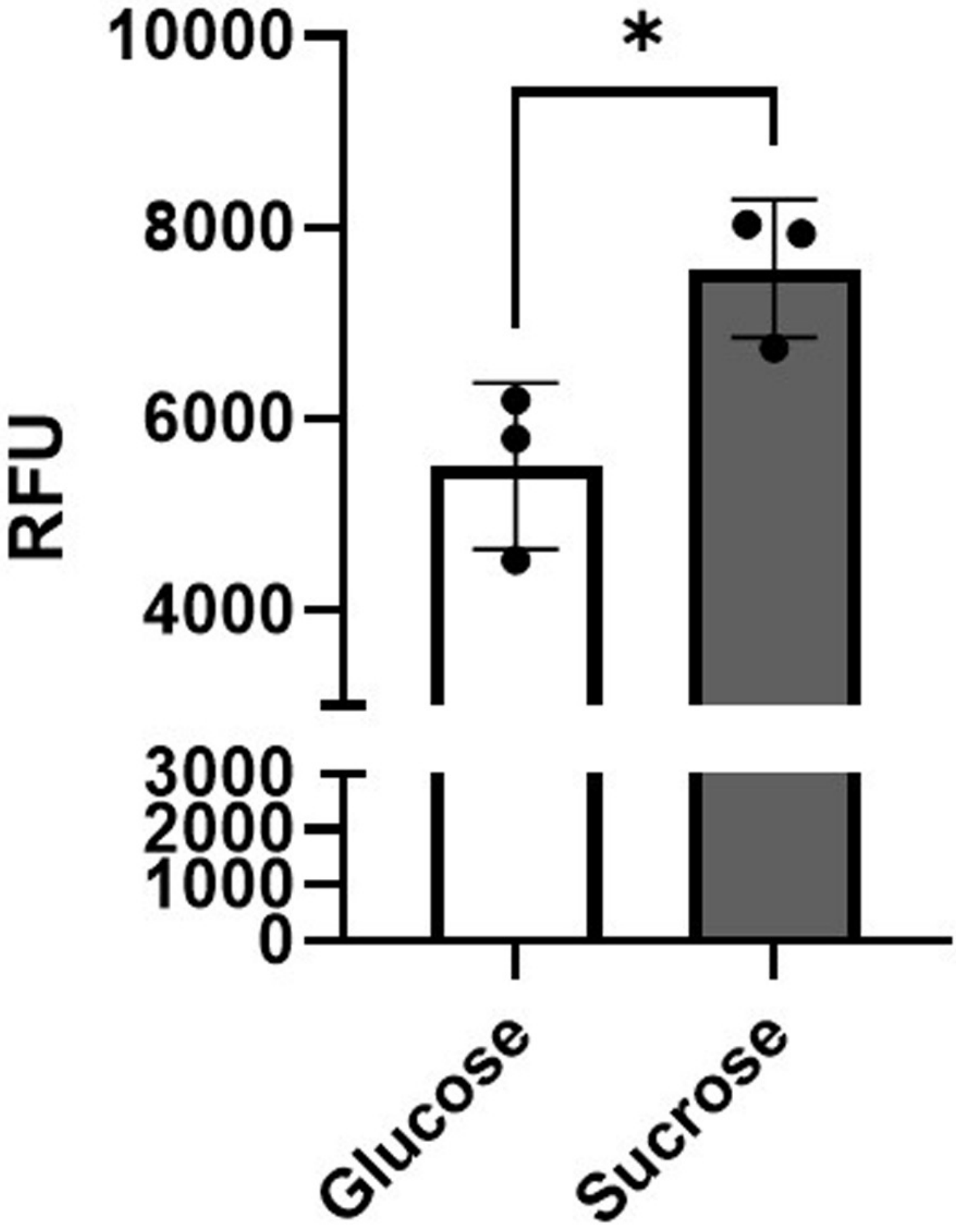
10000
8000
6000
4000
3000
2000
1000
0
RFU
*
Glucose
Sucrose

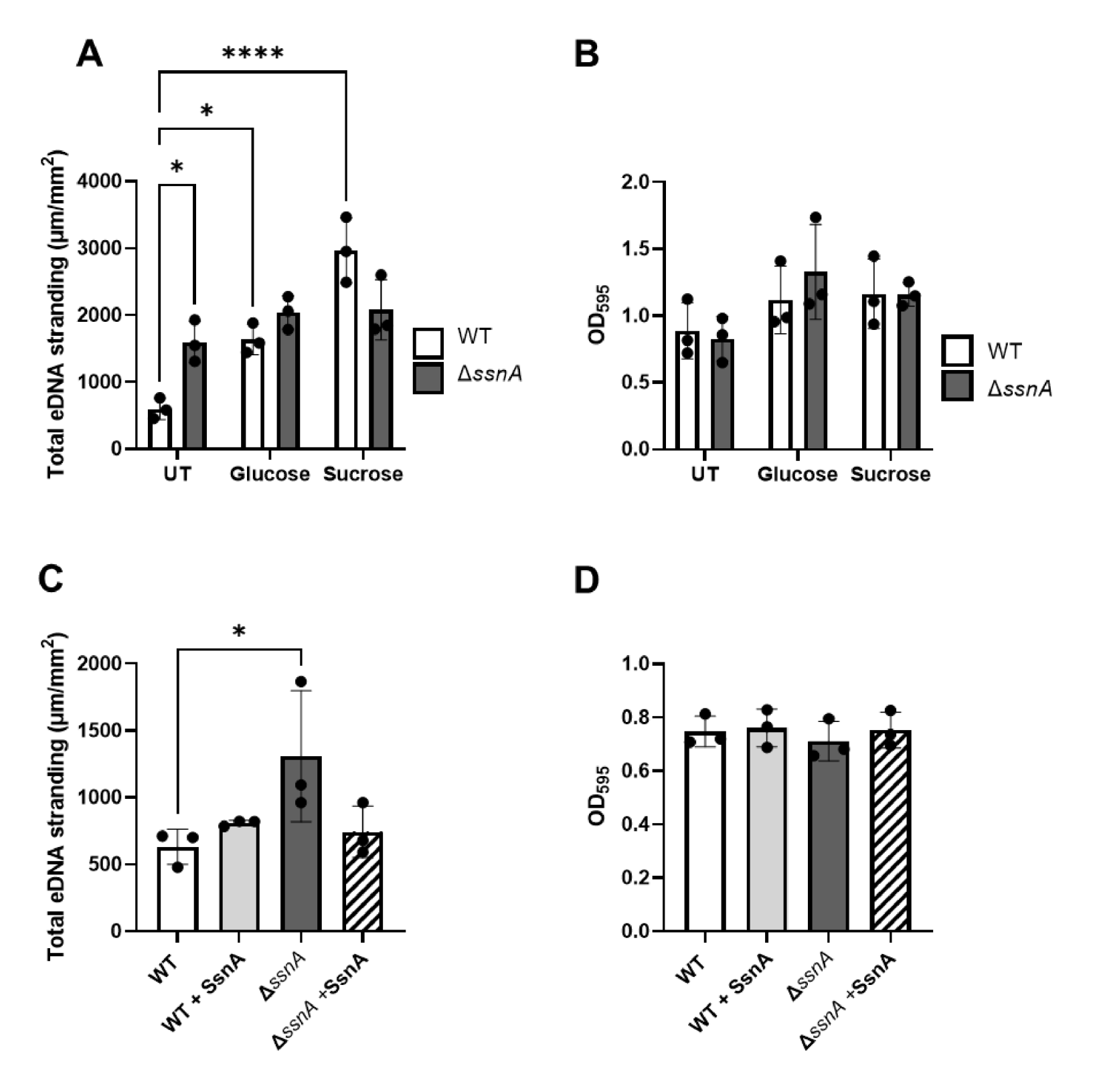
A
****
*
*
Total eDNA stranding (µm/mm²)
4000
3000
2000
1000
0
UT
Glucose
Sucrose
WT
ΔssnA
B
OD595
2.0
1.5
1.0
0.5
0.0
UT
Glucose
Sucrose
WT
ΔssnA
C
*
Total eDNA stranding (µm/mm²)
2000
1500
1000
500
0
WT
WT + SsnA
ΔssnA
ΔssnA +SsnA
D
OD595
1.0
0.8
0.6
0.4
0.2
0.0
WT
WT + SsnA
ΔssnA
ΔssnA +SsnA

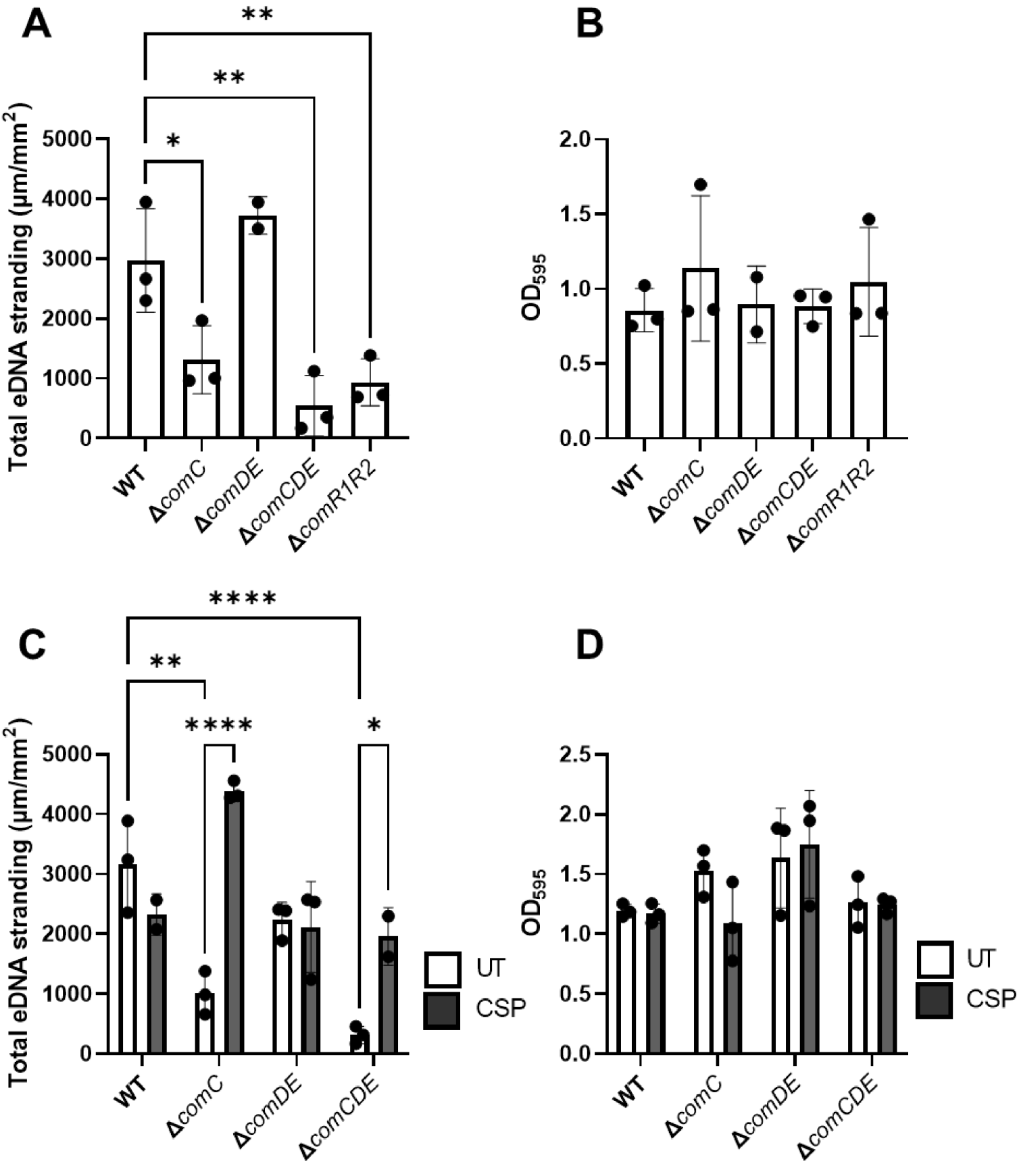
A
B
C
D
Total eDNA stranding (μm/mm²)
OD595
WT
ΔcomC
ΔcomDE
ΔcomCDE
ΔcomR1R2
UT
CSP
*
**
****

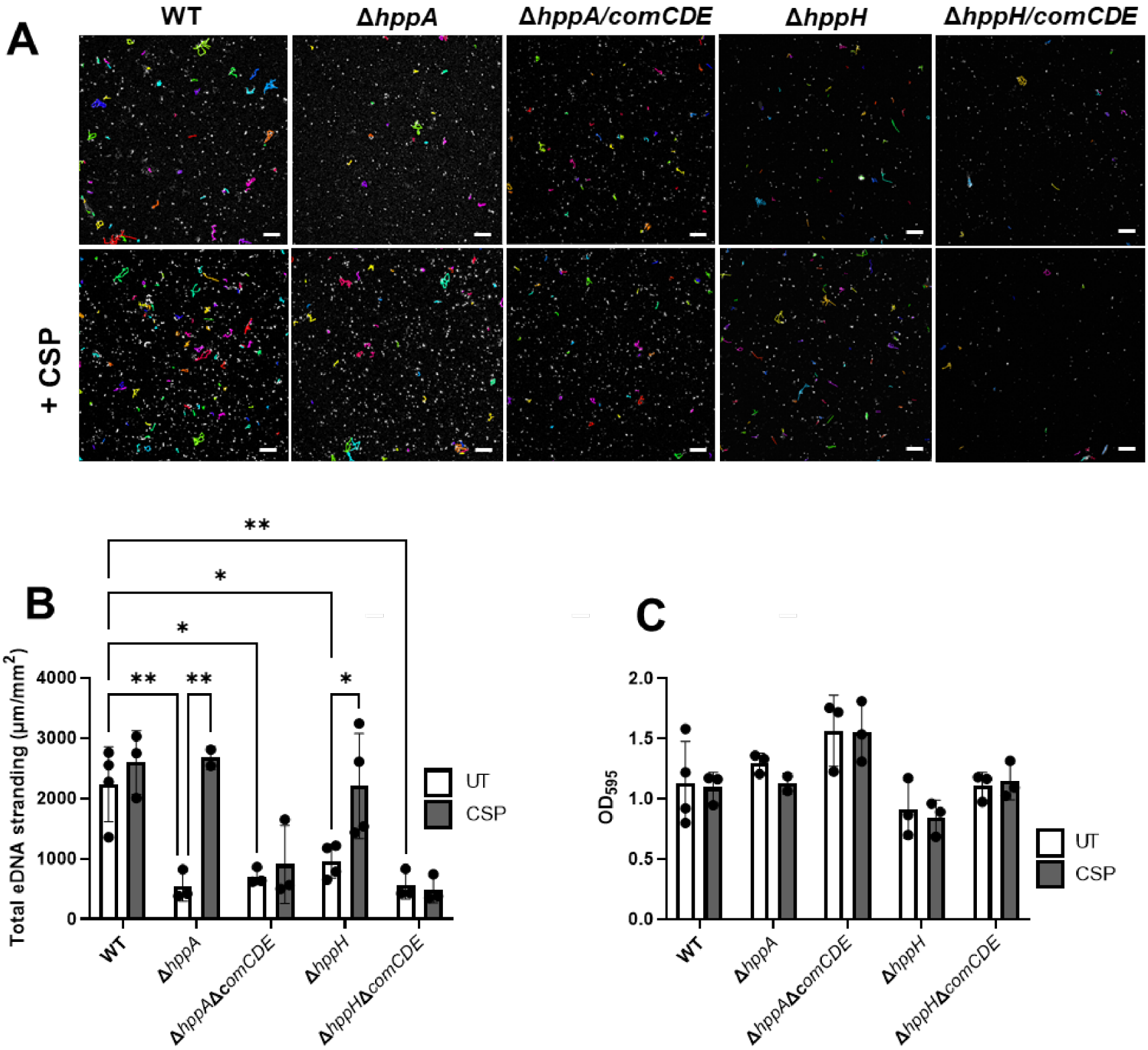
A
WT
ΔhppA
ΔhppA/comCDE
ΔhppH
ΔhppH/comCDE
+ CSP
B
Total eDNA stranding (µm/mm²)
4000
3000
2000
1000
0
**
**
*
*
*
UT
CSP
WT
ΔhppA
ΔhppAΔcomCDE
ΔhppH
ΔhppHΔcomCDE
C
OD595
2.0
1.5
1.0
0.5
0.0
UT
CSP
WT
ΔhppA
ΔhppAΔcomCDE
ΔhppH
ΔhppHΔcomCDE